THESIS

VULNERABILITY ASSESSMENT OF EXTENDED END-PLATE CONNECTIONS UNDER MAINSHOCK-AFTERSHOCK SEQUENCES

Submitted by

Risa Nicole Benvenga

Department of Civil and Environmental Engineering

In partial fulfillment of the requirements

For the Degree of Master of Science

Colorado State University

Fort Collins, Colorado

Summer 2018

Master's Committee:

Advisor: Hussam Mahmoud

Suren Chen
Bolivar Senior

ABSTRACT

VULNERABILITY ASSESSMENT OF EXTENDED END-PLATE CONNECTIONS UNDER MAINSHOCK-AFTERSHOCK SEQUENCES

After multiple seismic events in the mid 90s where welded connections performed poorly, bolted beam-to-column connections were investigated as a potential alternative. Extensive experimentation was performed to better understand the behavior of the joints, and models were developed in order to simulate their complex behaviors. The models included numerical finite element models, mathematical models, and mechanistic models. While all models have their limitations, mechanistic models have been shown to provide excellent balance between efficiency and accuracy in terms of analysis time and behavior prediction. In general, it has been shown than most models are able to accurately capture the behavior of the connections under monotonic and cyclic loading, representing the effect of mainshocks on connection behavior. However, research into the effects of mainshock-aftershock sequences that occur during many earthquakes on connection behavior has generally been lacking. Moreover, assessment of connection behavior, whether subjected to mainshock or mainshock-aftershock sequences, using a probabilistic framework has not received sufficient attention despite such analysis approaches being a basic requirement for performance-based engineering.

This study included two overarching goals. The first goal was to utilize mechanistic models for assessment of behavior of end-plate connections under mainshock-aftershock sequences. The second goal was to employ the developed models in probabilistic analysis for the development of fragility functions that describe the probability of exceeding a specific limit state of the connection

components for an increasing level of earthquake intensity. Specifically, for the first goal, two different strengths of extended end-plate connections were investigated. Component-based mechanical models in accordance with Eurocode 3 were developed to simulate the behavior of extended end-plate connections under mainshock-aftershock loading in this study. An understrength factor was developed in order to account for the inherent conservatism within Eurocode 3. For the second goal, fragility functions for the different failure modes and limit states, pertaining to the various connection components, were created based upon the results of a Monte Carlo simulation. The modulus of elasticity, yield strength, and ultimate strength were treated as random variables and the limits states evaluated included the bolts failing in tension, the column web failing in shear, and the exceedance of rotational limits.

The analysis results show that the most likely mode of failure was that of the bolts in tension. It was also observed that the aftershock ground motions had a larger effect on probability of failure for strength limit states, while the mainshock had a larger effect on the probability of failure for the rotational limit states.

ACKNOWLEDGEMENTS

A special thank you to my advisor Dr. Hussam Mahmoud who helped me with the direction of my research and for giving me the guidance I needed when I was stuck on how to troubleshoot my code. I don't know how I could have narrowed down my topic without his help and guidance.

Thank you to my friends for fielding my questions on MATLAB when I couldn't find an answer online. Thank you to Natalia, Caroline, and Matt for being my shoulders to cry on and walls for bouncing ideas, and for the late-night coffee and dinner runs. Without them, I could not have finished this thesis, communicated half as effectively or coherently as I did, or been as productive as I needed to be.

Thank you to Mr. Bear, who understood that sometimes "play time" meant sitting at my feet in a coffee shop chewing on a bone while I worked on research.

But most heavily, thank you to my mother and father. Without them, I would not have finished my thesis or even gone to grad school. They have encouraged me to grow and persevere even when all I wanted to do was run away. They have taught me the importance of keeping self-deadlines and helped to enforce them so that I would be done on time. They've listened to all of the successes and all of the failures and always pushed me to keep going.

TABLE OF CONTENTS

LIST OF TABLES

LIST OF FIGURES

1 INTRODUCTION

1.1 Problem Statement

During the 1994 Northridge and 1995 Kobe earthquakes, beam-to-column welded connections performed poorly, with inherent drawbacks in the geometry of the connection and in the force concentrations within the connection (Swanson and Leon 2000). Some of the failures were also due to the low toughness weld materials that were used, which led to cracking in the heat-affected zones of the welds. The connection geometry as well as the practices of field welding prior to the earthquakes also contributed heavily to the poor performance of the welded connections during seismic events (SAC 2000). This poor performance led to a push for exploring other alternatives for connections in steel structures in high seismicity regions.

The alternative most heavily investigated was the use of bolted connections instead of welded connections. Bolted connections were considered a viable option due to their internal redundancy and because they provide a comparable level of stiffness to that of welded connections. Additionally, bolted connections are cheaper to fabricate, faster to construct, and generally more consistent in their quality than welded connections (Murray and Sumner 2003; Swanson and Leon 2000).

In order to determine the viability of bolted connections, extensive studies were performed both experimentally and analytically to evaluate the behavior and characteristics of different bolted connection geometries. The most common types of bolted connections include T-stub connections, extended end-plate connections, and top-and-seat angle with double web angle connections (Mahmoud 2011). Extended end-plate connections, specifically their performance under seismic loading, are of particular interest to this study.

Bolted connections have been used extensively in Europe and have been subdivided into five categories based upon the tensile and shear loading that the connection is expected to undergo. These categories include: A) bearing type connections, B) slip-resistant at serviceability limit state, C) slip-resistant as ultimate limit state, D) non-preloaded connections, and E) preloaded connections. Categories A through C are governed more heavily by shear while categories D and E cover connections loaded in tension. Category E also includes moment-resisting connections as they may be loaded cyclically while category D only encompasses connections that can withstand monotonic loads. Various studies have been conducted to develop tools that would allow for accurate prediction of the behavior of the connections. These include mechanical models, mathematical models, and finite element models. Mechanical models have been developed and adopted by Eurocode 3 based upon the connection category as well as topology (CEN 2005).

Mechanical models have been used extensively for simulating the behavior of extended end-plate connections subjected to both monotonic and cyclic loading. Extended end-plate connections have been under investigation for their moment-resisting behavior, and have been shown to be a viable option for use in areas of high seismicity due to their stable performance under cyclic loading (Augusto et al. 2014, 2016; Ghobarah et al. 1990; Latour et al. 2011; Málaga-Chuquitaype and Elghazouli 2010; Simões da Silva et al. 2016). However, as noted in many studies, it is becoming imperative to look at the behavior of structures and their connections under sequences of cyclic loading so that not only the mainshock event of an earthquake is simulated, but aftershock events as well (Admuthe 2018; Li and Ellingwood 2007; Li et al. 2014; Mahin 1980; Ruiz-García and Negrete-Manriquez 2011). It has been shown that the aftershock event can actually cause more damage to the structure due to the deterioration of stiffness and reduction in strength that were caused by the mainshock.

There is very little research that has been conducted to account for the effect of mainshock-aftershock sequences on structural response. Moreover, the studies that have been conducted thus far considered structural response at the system level, with limited attention given to the behavior at the connection level. Thus, the investigation of the behavior of extended end-plate connections subjected to mainshock-aftershock sequences is both new and pertinent to the understanding of the effects of aftershocks on these connections.

1.2 Objectives and Scope of Research

In this study, the behavior of two extended end-plate connections subjected to mainshock-aftershock sequences were analyzed using component-based mechanical models following the guidelines from Eurocode 3 (CEN 2005). The primary objectives of this study were to compare the effects of the mainshock event to the aftershock event for each of the connections to determine which event was more detrimental to the connection. Additionally, the performance of the two different strengths of extended end-plate connections under the mainshock-aftershock sequence were compared to determine how the strength of the connections affects the performance under seismic loading.

The vulnerability of the connection to seismic loading was assessed through the creation of fragility curves for the different limit states, corresponding to the different components, of the connection subjected to mainshock-aftershock sequences. Limit states were defined based upon the AISC Extended End-Plate Design Guide (Murray and Sumner 2003) and the rotational limits set forth by Aksoylar et al. (2011) for classification of different global damage states. Unlike in previous studies, mechanical models have not been used to simulate connections under mainshock-aftershock sequences for the purpose of creating fragility functions.

The above objectives were realized using the following tasks:

1. Conduct a comprehensive literature review.
2. Develop a mechanical model for the connections of interest.
    i. Determine the applicable components for the extended end-plate connection following Eurocode 3 specifications.
    ii. Develop a 2D component-based mechanical model in MATLAB following the Eurocode 3 specifications.
    iii. Validate the monotonic and cyclic loading of the model against other studies that have been conducted on similar topics.
    iv. Develop and apply the understrength factor to the mechanical model to compensate for the conservatism of the Eurocode 3 model approach.
3. Conduct hysteretic moment-rotation analysis.
    i. Apply the rotations for the mainshock-aftershock sequences from Admuthe (2018) to the mechanical model.
    ii. Run multiple simulations over the same set of sequences with varying material properties within the model.
4. Create fragility functions for each limit state.
    i. Determine the limit states from Murray and Sumner (2003) that are applicable to the mechanical model.
    ii. Develop probabilities of exceeding the given limit state for each spectral acceleration for the mainshock-aftershock sequence, mainshock event, and aftershock event.
    iii. Fit fragility functions to each of the exceedance probability data.

5. Assess the effects of mainshock vs aftershock ground motions and connection strength.

1.3 Organization of the Dissertation

This thesis includes five chapters. Chapter 1 introduces the problem statement as well as the objectives of the study, scope of work, and organization of the thesis. Chapter 2 is an extensive literature review including information on extended end-plate connections, existing models for use in representing the connections, and the creation and use of fragility functions, which were developed to assess the performance of the connections. Chapter 3 details the methodology used for modeling the extended end-plate connections with component-based mechanical models, the development of the understrength factor to account for the inherent conservatism in the Eurocode 3 modelling approach, and the development of the fragility functions based upon limit states outlined in the AISC design guide. The results of all of the analyses are presented in Chapter 4, specifically the fragility functions developed for bolts failing in tension, column web failing in shear, and rotation exceeding the defined limits. Additionally, comparisons between the two connection strengths and comparisons between the mainshock and aftershock events are included. In Chapter 5, the study is summarized and the conclusions from the study are presented.

2 LITERATURE REVIEW AND BACKGROUND

2.1 Mainshock-Aftershock Sequences

In seismic design, engineers are most often concerned with the demands on the structure due to a single earthquake. However, earthquakes are very rarely an isolated event; in most cases there are smaller ground motions in the same area and within a particular timespan that are considered to also be a part of the seismic event. These ground motions are referred to as foreshocks when they occur before the mainshock event, and aftershocks when they occur after the mainshock event. In both cases, the magnitude of the mainshock is the largest of the ground motions, but it is possible for the peak ground acceleration to be larger or the duration longer in a foreshock or aftershock (Abdelnaby 2012; Admuthe 2018).

It has been observed that aftershock effects can often cause greater amounts of damage than the mainshock due to the loss of strength and/or stiffness that a structure undergoes during the mainshock. Slight damage from a mainshock event can lead to more severe damage in any subsequent ground motions that may occur (Admuthe 2018). One such example can be seen in Figure 2-1, which depicts on the right a reinforced concrete structure after the mainshock of the Gediz earthquake on March 28, 1970, and the same structure after the subsequent aftershock for the same earthquake on the left. It can be seen that while the damage to the structure due to the mainshock has caused a considerable amount of drift at the second level, the second floor was still standing. In the aftershock figure, the second story has completely collapsed (Abdelnaby 2012).

Figure 2-1. Reinforced concrete structure before and after the aftershock event from (Abdelnaby 2012)

One of the early works that considered the effects of the mainshock-aftershock sequence rather than just the mainshock was conducted by Mahin (1980) using single-degree-of-freedom (SDOF) systems. The results indicated a higher structural ductility after the aftershock than the mainshock.

Song et al. (2014) investigated the influence of duration and frequency content of earthquakes on structures that had already been subjected to a mainshock earthquake. It was concluded that structures with greater amounts of damage after the mainshock are more susceptible to collapse during an aftershock.

Ruiz-García and Negrete-Manriquez (2011) evaluated the effects of as-recorded and simulated aftershocks on steel-frame buildings. It was determined that the artificial seismic ground

motions overestimated drift demands and the recommendation that the as-recorded aftershock sequences should be used when assessing potential damage to existing structures was made.

Li and Ellingwood (2007) investigated the potential for additional damage to a steel moment frame to occur during an aftershock event. Damage was measured using the maximum inter-story drift ratios and a normalized damage ratio defined by the authors. The study focused on steel moment frames with welded connections and found that damage due to the aftershocks was a function of the characteristics of the aftershock and the damage accumulated during the mainshock event. It was also determined that even if the damage from the mainshock was small, it could lead to a large damage ratio from the aftershock.

Li et al. (2014) evaluated the collapse fragilities of steel structures during aftershocks for use in performance-based engineering. The resulting fragility functions were intended for use with the aftershock ground motions in order to estimate the collapse potential during aftershock events.

Admuthe (2018) investigated the effects of different fundamental periods of structures on steel moment frames subjected to as-recorded mainshock-aftershock sequences. The resulting drift fragilities and period elongation of the structures were considered and a relationship between the connection capacity of the frames and the period elongation was observed.

It should be noted that while mainshock-aftershock sequences have been investigated, all of the studies have focused on frame-level assessments of various aspects of the sequences. Currently, there are no studies that focus on the connection level impacts of mainshock-aftershock sequences. Undoubtedly, fragility functions for exceeding the connection rotation limit states could be developed using the output of the frame analysis from Admuthe (2018). However, these fragilities alone, while useful, do not provide information on the failure probability of the various components that comprise the connection. The importance of these detailed fragilities lies in their

potential use in a detailed performance-based engineering framework where losses associated with connection damage can be accurately computed since the probability of damage to each component is properly quantified.

2.2 Extended End-Plate Connections

Extended end-plate connections are moment-resisting connections, which consist of an end plate welded to the end of a beam and connected to another beam-end plate configuration or to the flange of a column, typically with four or eight bolt rows. These connections typically have two bolts per row located on either side of the beam web, and one or two rows on either side of the beam flange. The end plate may or may not have stiffeners to increase the strength of the connection, and the same is true for the column web. Variations of this type of connection are shown in Figure 2-2.

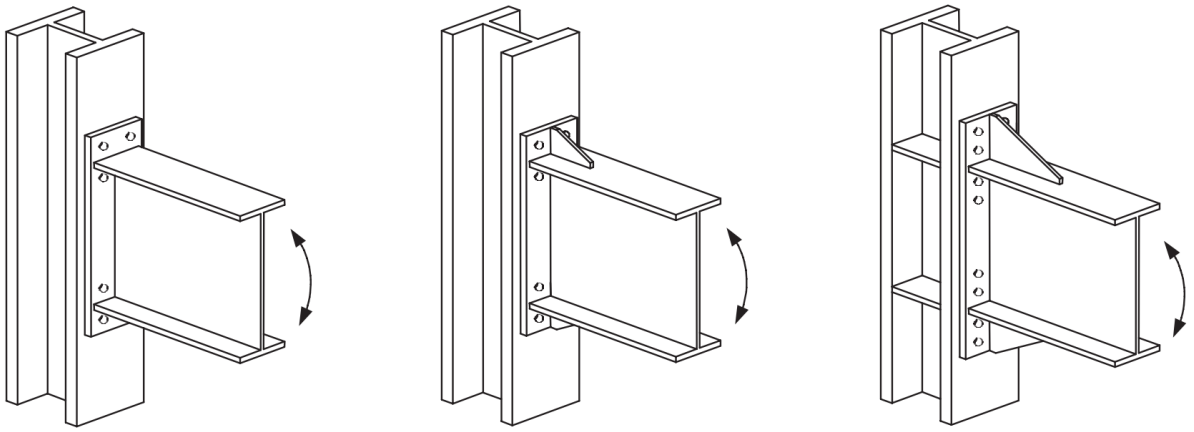

(a) Four Bolt Unstiffened, 4E *(b) Four Bolt Stiffened, 4ES* *(c) Eight Bolt Stiffened, 8ES*

Figure 2-2. Extended End-Plate Connection under investigation (Murray and Sumner 2003)

According to the AISC Steel Design Guide for Extended End-Plate Moment Connections for Seismic and Wind Applications (Murray and Sumner 2003), there are multiple advantages and

disadvantages to the use of end-plate connections. The two major advantages are the competitive installation cost for most cases and the relatively fast erection process. These stem from the ability of the connection to be erected during the winter since only bolting must occur in the field, as well as the ability to perform all necessary welding in the shop. This eliminates problems associated with field welding. Additionally, if the fabrication is performed correctly, these connections maintain the plumbness of the frame. Conversely, there are stringent fabrication requirements to ensure that the beam ends are square to the column. While the in-shop welding avoids field abnormalities, the end plates often warp due to the heat from the welding, which can introduce residual stresses into the connection, and the end plates are also subject to lamellar tearing near the flange welds when tensile loading occurs. The additional prying forces due to the pretensioning of the bolts must be checked and included in the strength calculations for the connection (Murray and Sumner 2003). These connections have been extensively evaluated experimentally (Abidelah et al. 2012; Ghobarah et al. 1990; Girão Coelho et al. 2004; Latour et al. 2011; De Lima et al. 2002; Prinz et al. 2014; Pucinotti 2001; Del Savio et al. 2009; Shaker and Abd Elrahman 2014). All of these studies demonstrate the connection capacity for moment resistance. Some of the more recent studies applicable to earthquake loading are discussed below.

Ghobarah et al. (1990) was one of the first to conduct experimental tests on bolted extended end-plate connections under extreme cyclic loading. The goal of the work was to better understand the behavior of the connection and assess the effects of different components on the overall behavior. It was found from the test results on five different connections that excellent ductility and load-carrying capacity could be achieved under cyclic loading, which supported the use of extended end-plate connections in high seismic regions.

Girão Coelho et al. (2004) tested eight different statically loaded extended end-plate connections in order to better understand the behavior of the connection up to and including failure. The effects of end-plate thickness and steel grade were considered during testing. The experimental data revealed that an increase in the end-plate thickness corresponded to an increased moment resistance and initial joint stiffness. The rotational behavior and capacity of the joints were also an important part of the study as these characteristics are necessary for seismic design. It was found that the Eurocode 3 rotation limits provided were extremely conservative when compared to the actual rotational capacity of the joints tested experimentally.

Prinz et al. (2014) noted that some extended end-plate connections were designed such that retrofitting or repair might be necessary after an earthquake and proposed the use of thicker end plates and additional bolts per row during design and initial construction as solutions to avoid the need for retrofitting or repair. It was found that increasing the number of bolts per row increased the moment capacity of the connection, but that bolt prying forces increased as bolts drew closer to the column web centerline. It was also determined that thicker end plates increased the moment capacity but also increased the difficulty of construction because the end plates were not as easily bolted to the column.

2.3 Models for Predicting Connection Behavior

2.3.1 Mathematical Models

Mathematical models were developed to provide an approximation of moment-rotation behaviors by first testing the connection in question. Frye and Morris (1975) proposed one of the earliest mathematical models, which determined the rotation of the connection based upon the moment and curve-fitting parameters. The curves were fitted to the following odd-power

polynomial equation assuming monotonic loading, shown in Equation 2-1. This equation was found to have reasonable agreement with the actual moment-rotation relationship.

$$\theta_r = C_1(KM)^1 + C_2(KM)^3 + C_3(KM)^5 \qquad \textit{Equation 2-1}$$

where θ_r = the rotation

M = the moment

C_1 , C_2 , C_3 = curve fitting parameters

K = a standardized parameter based upon the geometric characteristics of the connection

An alternate equation was proposed by Richard and Abbott (1975) for the moment-rotation curve under monotonic loading using a three-parameter power model that followed Equation 2-2. This equation required prior knowledge of the connection stiffness and plastic rotation in order to properly model the connection.

$$M = \frac{R_{ki}\theta_r}{\left[1 + \left(\frac{\theta_r}{\theta_0}\right)^n\right]^{\frac{1}{n}}} \qquad \textit{Equation 2-2}$$

where θ_r = the rotation

M = the moment

R_{ki} = the initial connection stiffness

n = the shape parameter

θ_0 = the reference plastic rotation

Additional mathematical models have been created over the years (Ang and Morris 1984; Kishi and Chen 1990; Lui and Chen 1986). These models consisted of a general equation that was fitted to experimental results. This created an approximation of the behavior based upon previous

experimental behavior for a specific connection, but these models were not applicable to any size or type of connection. Each curve fitting procedure and set of parameters was only applicable for connections of the same size and the configuration of the connection that was used for fitting. Additionally, these models were only developed for monotonic and static loading. Leon et al. (2004) conducted tests to compare some of the mathematical models to the cyclic behavior of connections. It was demonstrated that these models did not accurately simulate the connection behavior under cyclic loading, and therefore these models are not appropriate for the current study.

2.3.2 Mechanical Models

The introduction of mechanical models for use in joint representation occurred to help assimilate joint response into frame analysis. It was considered more broadly applicable than mathematical models because each of the components was modelled based upon the mechanical properties of that component, and thus was applicable to more connections than the experimentally-based mathematical models. Mechanical models can also be used for the determination of the rotational capacity in partial-strength joints.

A mechanical model based upon Eurocode 3 (CEN 2005) is generally a simplified 2-dimensional component-based spring model that simulates the behavior of a beam-to-column joint. The components of a mechanical model each represent a region of the joint that has a specific behavior and are often divided into 3 zones based upon the type of loading that is experienced: tension, compression, and shear.

Component models are made up of springs and rigid links based upon whether the component in question is deformable or not. Generally, rigid links are used to connect parallel springs along different bolt lines. Springs represent the components of the joint that resist the

loading that is undergone. Eurocode 3 Part 1.8 (CEN 2005) has a comprehensive list of the possible components within a joint as well as the loading that is undergone. For example, the column web in shear and the column web in transverse compression are represented by two separate springs due to the differences in behavior caused by the different loading. The general rule of thumb is that components that experience the same force are configured in series, while components that undergo the same displacements are configured in parallel. For example, components along the same bolt line are in series. These components represent pieces of the joint, such as the column web in compression or the column flange in bending. A typical component-based mechanical model is seen in Figure 2-3, with (a) demonstrating a three-bolt extended end-plate connection and (b) illustrating the corresponding mechanical model (Girao Coelho et al. 2006; Pucinotti 2001).

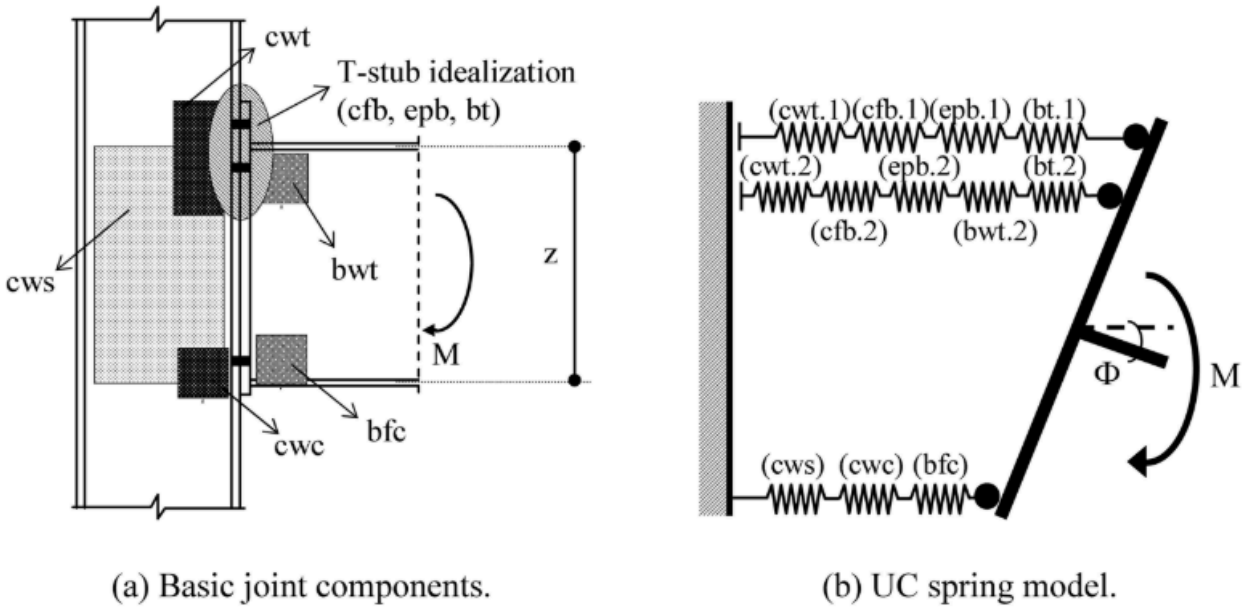

Figure 2-3. Typical component-based mechanical model from Girao Coelho et al. (2006)

The creation of mechanical models can be explained in four major steps. First, the joints must be characterized based upon the rotational stiffness, resistance, and ductility. Once characterization has occurred, the joint can be modelled for representation within the actual frame

analysis. Joint classification as rigid, semi-rigid, or pinned is required to ensure that the correct boundary conditions are applied to the model at the component as well as the whole. Lastly, joint idealization is performed, which is to create a simplified behavior that sufficiently approximates or estimates the actual behavior of the joint (Jaspart 2000).

The first step in joint representation is based upon the component method outlined within Eurocode 3 (EC3) Part 1.8 (CEN 2005). The process for creating a mechanical model is to first determine the so-called "active" components in the joint. Not all components contribute to the rotational behavior of the joint, such as the beam flange and beam web in compression, as stated by EC3 Part 1.8 in Table 6.11 (CEN 2005). Once the active components have been identified, the components are characterized using force-deformation curves (generally a linear elastic-perfectly plastic or bi-linear approximation) to simulate the individual behaviors of the components. An example of this approximation can be seen in Figure 2-4. EC3 outlines the values to be used for the stiffnesses and the strengths of each component. The components are then assembled to create the mechanical model. Components that undergo displacements are represented by springs and arranged along the bolt lines. In the case where a zone (tension, compression, or shear) overlaps two bolt lines, the tributary area is split such that the one component is represented by two springs – one along each of the bolt lines. This occurs when there are two bolt rows in tension or compression and happens with the column flange in bending, column web in tension, and the end plate in bending (Girao Coelho et al. 2006; De Lima et al. 2002).

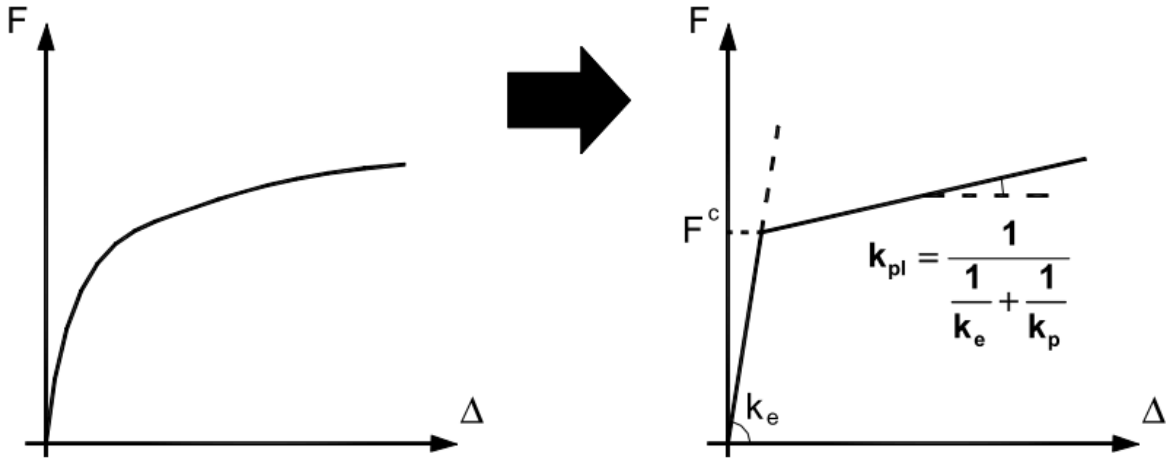

Figure 2-4. A bi-linear behavior approximation uses in the component-based mechanical models from De Lima et al.(2002)

In the case of the extended end-plate connection, the tension zone of the joint can be idealized as a series of equivalent t-stubs according to EC3. During calculation, each component is assumed to be connected to a rigid foundation, which allows for full strength development of the specimen. The behavior of the t-stubs can be approximated as bi-linear with the initial stiffness calculated following Section 6.2.4 from Eurocode 3 Part 1.8 (CEN 2005). Additionally, when the t-stub strengths are calculated, the bolt strengths are accounted for in the resistance of the equivalent t-stub. However, non-zero values for the post-yield stiffness are calculated based upon a method determined by Jaspart as the Eurocode assumes elastic-perfectly plastic behavior (Girao Coelho et al. 2006). This use of the Eurocode provides the joint component idealization that is the last step for the representation of the joint. Once this has been completed, the model can be used to predict the behavior of the joint as a whole based upon the interactions of the individual behaviors of the components within the joint.

The method of component based mechanical models for design and analysis of the strength of joints can be applied to any joint and any loading scenario – in theory. In practice, component-

based models are used for the rotational capacity of a joint. With multiple different assembly procedures for the mechanical model, it is important to note that the rules for model assembly commonly used at the University of Coimbra (referred to as the UC model) were utilized for the analysis of all joints within this study (Girao Coelho et al. 2006).

Pucinotti (2001) focused on a comparison between the Eurocode 3 Annex J approach and experimental testing for the prediction of behavior of top-and-seat and web angle connections and the creation of an even simpler model for use for this connection. Annex J is a supplement to Eurocode 3 Part 1.8, which specifies additional information for particular types of connections such as top-and-seat connections. Characterization of the components for the mechanical model followed the procedures outlined in Eurocode 3, resulting in bi-linear approximations of the stiffnesses and strengths of each component. The resulting predicted behavior of the entire system had a much lower strength than the experimental results. In almost all cases, the experimental data and the mechanical model were in agreement of initial stiffness of the connection, while the yield point and ultimate strength predicted by the model were approximately one-half to one-third the magnitude shown by the experimental results. The conclusions reached by this paper were that Annex J of Eurocode 3 did not accurately represent the strength and deformation capacity of the joints examined, which is illustrated in Figure 2-5. However, it should be noted that the Eurocode was created for the purpose of design, not research and therefore the prediction being lower than the actual capacity would be considered as conservative and potentially acceptable for the purpose it was created.

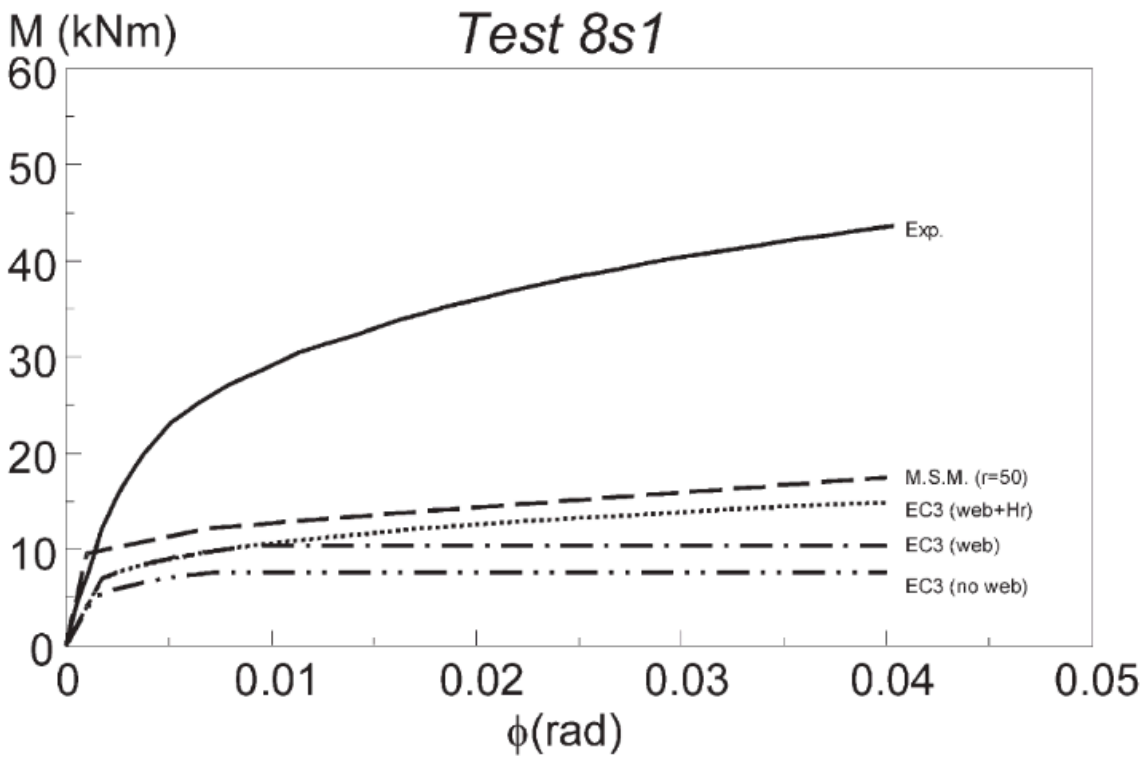

Figure 2-5. Comparison of experimental results to EC3 component-based mechanical models from Pucinotti (2001)

De Lima et al. (2002) compared a mechanical model of a beam-to-column semi-rigid joint to a 3-D finite element analysis of the same joint to determine the agreement between the two methods. The mechanical model was first validated against experimental tests run previously to ensure that proper behavior was occurring within the model. The standard characterization of the components with a linear elastic-perfectly plastic strength curve as specified by EC3 was used for the mechanical model, while the von Mises yield criterion was used to determine a tri-linear relationship for material non-linearity in the finite element model to determine whether the simplified behavior curve affected the final predicted behavior. In addition to a comparison between models, the column thickness was changed between runs to observe how it affected the strength of the connections. It was concluded that both the mechanical model and the finite element

analysis had acceptable agreement with the experimental results, and that the column thickness did greatly affect the joint strength and stiffness.

Girao Coelho et al. (2006) used extended end-plate connection tests from a ductility assessment experiment as a comparison to the UC spring model configuration to determine the accuracy of the model. The connection was broken into the three zones (tension, compression, and shear) and then components were assigned springs by bolt row following the procedures outlined in Eurocode 3. The determination of the accuracy of the T-stub idealization of the tensile components was the main focus of the research, which compared the spring model simplifications with the actual behavior of the yielding components. The 3D effects of prying mechanisms caused by loading were discussed and it was determined that the 1D effects accounted for in EC3 were acceptable for modeling. Instead of using the elastic-perfectly plastic behavior assumption given by EC3, the widely accepted bi-linear approximation outlined by Jaspart (2000) was followed, which gives the components a reduced stiffness after yield is reached. It was concluded that the use of the mechanical model for overall moment-rotation capacity was fairly accurate when the UC model configuration and the tri-linear component behavior approximation were used. It was also noted that the EC3 provisions were more conservative than necessary for the rotational capacity of joints.

The component-based mechanical model, as presented in Eurocode 3, is not meant for use in the prediction of connection behavior under cyclic loading. There have been several studies conducted that explore methods for adapting mechanical models for use in developing hysteretic loops for connections.

Simões da Silva et al. (2009) investigated calibrating the cyclic behavior of particular components to experimental data in order to reproduce the stiffness and strength degradations that

may be present. The mechanical model was simplified to only include the components of the end-plate connections that were deemed critical to the cyclic performance – in this case the column web panel in shear and the end plate in bending. All other components were assumed to be linear elastic for the entire loading cycle. The strength and stiffness were then calibrated to experimental tests of the individual components and applied to the model for simulations. Acceptable agreement between the modified mechanical model and experimental data for the connection tested were produced; however, comparisons were only made for one connection, which did not validate the model for use with other connection sizes or types. Additionally, experimental data was necessary to calibrate the degradation parameters of the components, which could pose a problem when experimental data is not available.

Latour et al. (2011) applied energy dissipation concepts to the component models under cyclic loading. The model was simplified into a single row of mechanical components for each side of the neutral axis and only the dissipative elements – column flange in bending, column web loaded axially, column web in shear, and the end plate in bending – were modelled cyclically, while all other components were considered to act linear-elastic to failure. Energy dissipation was used to determine the strength and stiffness degradation where applicable, and there was acceptable agreement between experimental and analytical results, as seen in Figure 2-6. However, the model is extremely sensitive to fabrication processes, which were not always available.

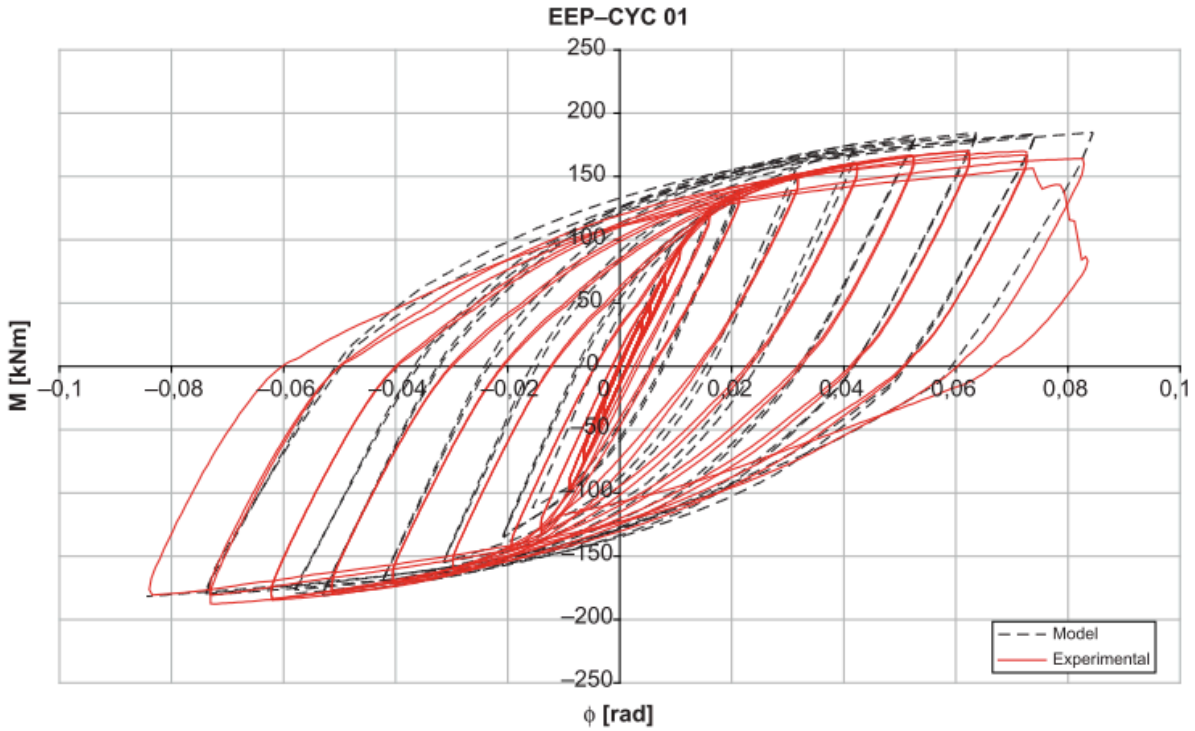

Figure 2-6. Comparison of experimental data to cyclic mechanical model from Latour et al. (2011)

Simões da Silva et al. (2016) discussed a process for determining the critical components within a connection using the monotonic loading of the component model to determine the yielding sequence. Only the critical components were modeled using cyclic behavior calibrated to experimental results. In order to create a fragility function, it was important to first have a large data set of values so that the probabilities of failure are as accurate as possible, which was feasible with mechanical models as they are very computationally inexpensive.

Limitations of the mechanical model include the inability to properly represent the local behavior that may occur during the loading and unloading process. Additionally, any permanent physical deformation, such as the curling of the end plate away from the column flange, cannot be modeled with mechanical springs. When these behaviors are of concern to the study, finite element models are often better suited.

2.3.3 *Finite Element Models*

Another option for modelling of extended end-plate connections when more detailed information and predictions are necessary is finite element models. These can be either 2-dimensional or 3-dimensional models and often allow for nonlinear behavior to occur. Several 3D finite element model studies where bolted connections were under investigation are presented below.

De Lima et al. (2002) investigated the behavior of minor axis beam-to-column semi-rigid connections experimentally in order to then develop finite element and mechanical models. A series of tests using a cantilever loading beam were compared to a finite element model of the column for the top-and-seat web angle connection, shown in Figure 2-7a. The model type used were eight-node shell elements. As can be seen in Figure 2-7b, there is excellent agreement between the finite element model and the experimental data.

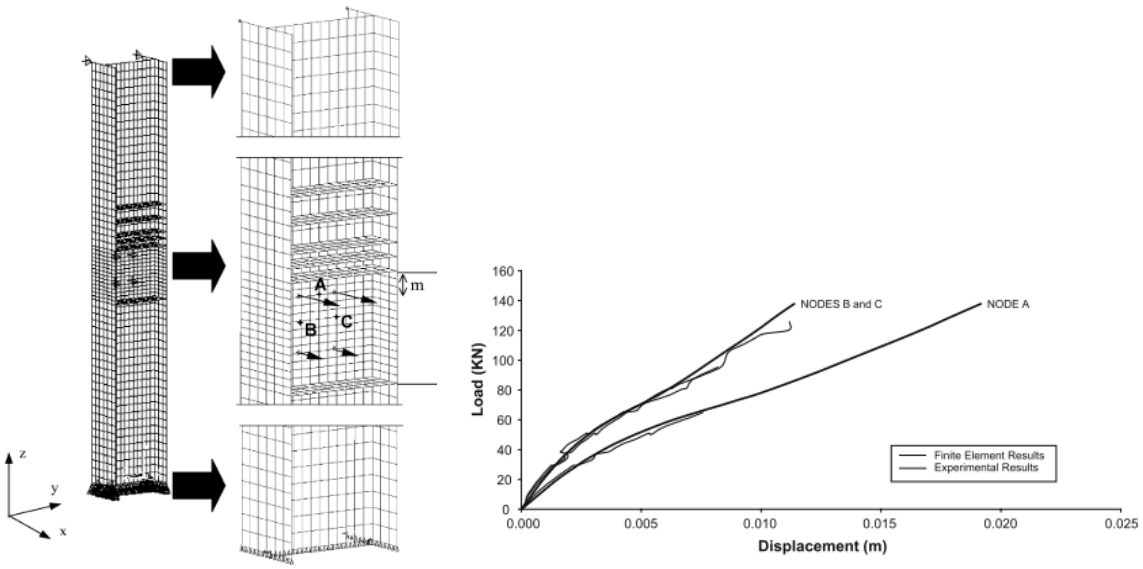

a) Finite element model *b) Comparison of finite element model results to experimental*

Figure 2-7. Finite element model and results from De Lima et al. (2002)

Baei et al. (2012) compared a finite element model of extended end-plate connections and to the Eurocode 3 component-based mechanical model to determine the level of agreement between the two different model types. The experimental data included loading of the connections with both a moment and axial load in order to test the differences between the finite element model and the component-based model. As can be seen in Figure 2-8, which shows the results of both the finite element results for different eccentricities on the axial loading as well as the EC3-based component model, the finite element models are more refined and show a greater range in strengths depending upon the location of the axial load, while the EC3 model was unable to account for the added force and moment from the axial load.

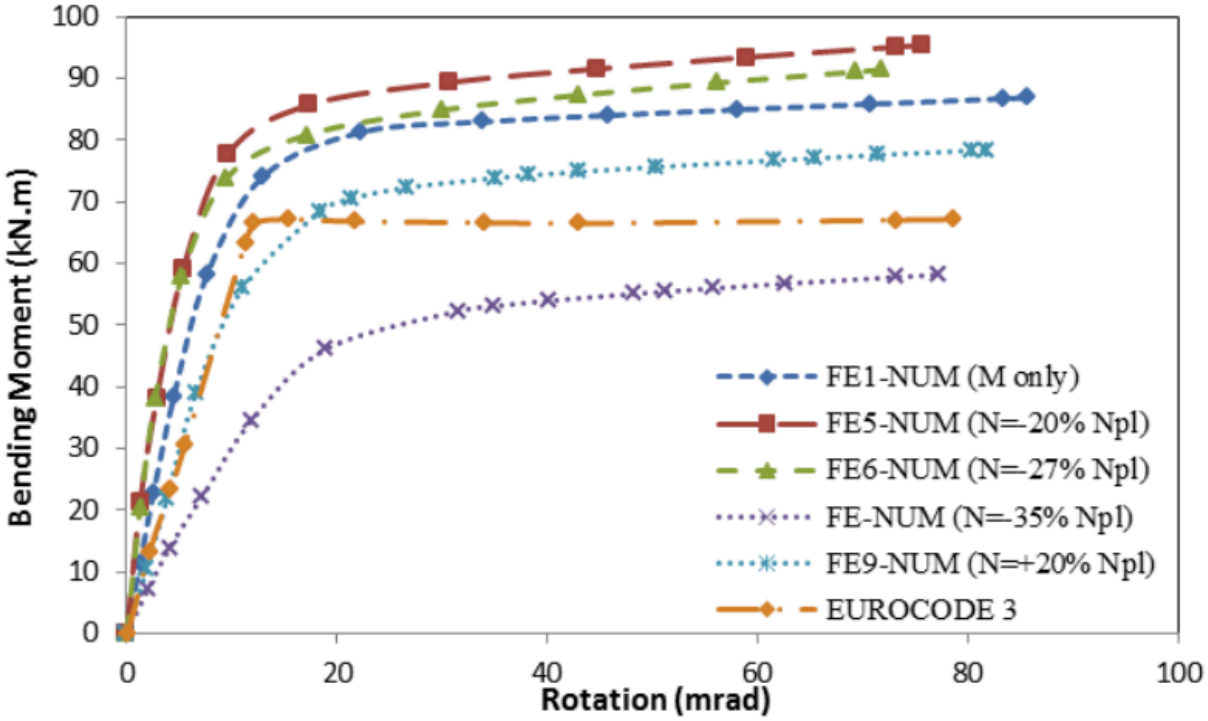

Figure 2-8. Comparison of finite element model to EC3-based component model from Baei et al. (2012)

Shaker and Abd Elrahman (2014) also investigated the effects of combined axial loading and bending on extended end-plate connections by creating finite element models that used

nonlinear eight-node solid structural elements. The models were found to have good agreement with experimental results, including permanent deformations at the bolt connection faces, as seen in Figure 2-9, where (a) depicts the deformation that occurred during experimental testing and (b) depicts the estimated deformation from the finite element (FE) model.

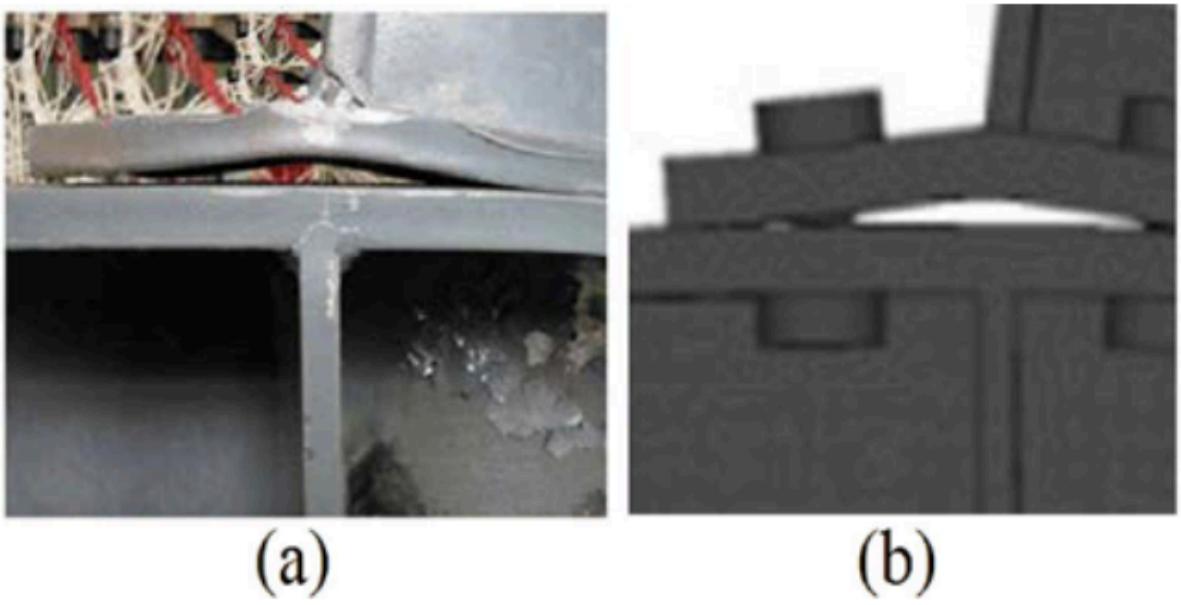

Figure 2-9. Comparison of experimental and FE simulated deformations from Shaker and Abd Elrahman (2014)

Augusto et al. (2016) created FE models of moment-resisting bolted connections in order to extract the necessary force-deformation responses of the different connection components under cyclic loading. These responses were then used to formulate a simpler mechanical model, but first the FE model had to be developed and validated. As seen in Figure 2-10, the FE model comprised of eight-node solid elements had good agreement with experimental data for the moment-rotation relationship.

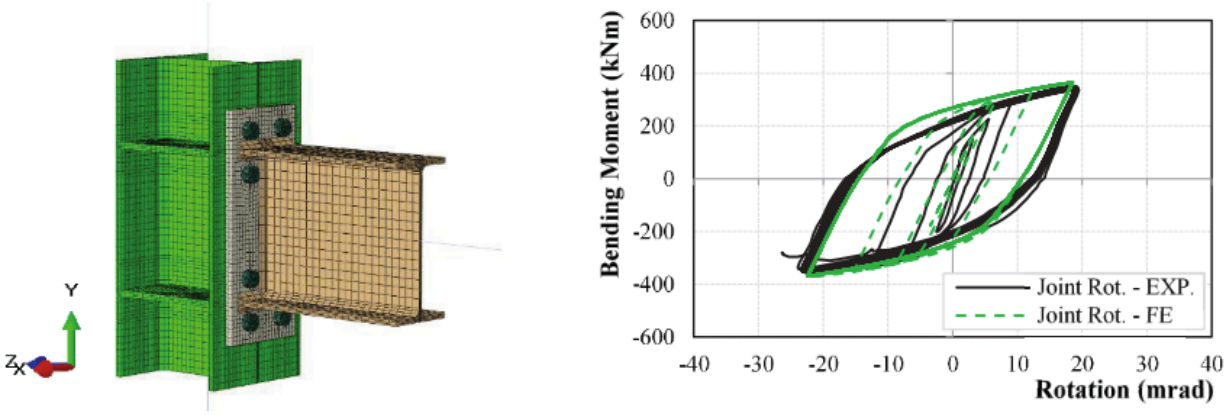

Figure 2-10. FE model and cyclic results from Augusto et al. (2016)

Finite element (FE) models overall have the detail and accuracy to predict the behavior of extended end-plate connections when the necessary computational power and time are available. FE models require large amounts of computing power to run and often take hours to process one simulation. In many cases, this is an acceptable compromise for the results that are extracted. However, in some cases, such as the development of fragility functions, it is necessary to run hundreds or thousands of similar simulations with the same model. In such situations, the use of a finite element model may not be the most economical choice for the study.

2.4 Fragility Functions

Building performance and seismic risk assessment are often evaluated using fragility functions, which describe the probability that a structural will fail to meet the performance objectives set forth in design (Ellingwood et al. 2007). A fragility function is defined broadly as a mathematical function that expresses the probability that some undesirable event occurs as a function of some measure of environmental excitation (Porter 2018). They are most commonly

represented by a lognormal cumulative distribution function (CDF) that takes the form shown in Equation 2-3.

$$F_d(x) = \Phi\left(\frac{\ln\left(\frac{x}{\theta_d}\right)}{\beta_d}\right) \qquad \textit{Equation 2-3}$$

where $F_d(x)$ = the fragility function for a damage state, d, evaluated at a particular value of the uncertain excitation, *x*

$\Phi(s)$ = the standard normal cumulative distribution function evaluated at *s*

x = a particular value of the uncertain excitation

θ_d = median capacity of the design in question to resist the damage state, d

β_d = standard deviation of the natural logarithm of the capacity of the design to resist the damage state, d

Once a fragility function has been fitted to Equation 2-3, the future performance of the structure or connection may be predicted for a given set of ground motions based upon the parameters listed.

Ellingwood et al. (2007) developed fragility functions for typical steel and reinforced concrete structures located in the central United States during seismic events. These fragility functions were then compared to the damage loss calculation software HAZUS to give an idea of the accuracy of the software.

Li et al. (2014) developed fragility curves for a four-story moment-resisting steel frame subjected to mainshock-aftershock sequences. The findings suggested that the damage and potential for collapse of the structure were more dependent upon the mainshock intensity than the aftershock intensity.

Attary et al. (2016) developed fragility curves for the three-story moment-resisting steel building outlined in FEMA-355C, which was subjected to tsunami loading. The fragility curves were created in terms of the momentum flux of the tsunami waves as well as the flow depth and the flow velocity to determine the probability of failure of the structure.

Hassan and Mahmoud (2018) developed fragility curves for hospitals following seismic events as part of the estimation of hospital functionality. In order to determine the functionality of the hospital, the probability of little to no damage sustained was first necessary.

Admuthe (2018) developed fragility functions for three moment frames during mainshock-aftershock sequences, which varied the connection strength to determine the effects on the performance of the structure as a whole. Connections with moment resisting capacities equal to 50%, 60%, and 70% of the plastic moment of the connecting beam were tested, but fragility functions were developed for the structure as a whole.

In order to create a fragility function, it is important to first have a large set of data so that the probabilities of failure are as accurate as possible. In order to reduce time for the creation of a dataset, it is valuable to use a mechanical model over a finite element model if the required data can be produced with the simpler model. While there are limitations to the mechanical model, such as not loading the model perpendicular to the spring lines, and the inability to model local behavior and deformations, the purpose of this work was to create fragility functions based upon limit states that can be modelled with the use of the mechanical model. For this reason, the reduction in computational power associated with the use of mechanical models and the reduction in time were considered to be more beneficial than the additional information available with the use of a finite element model.

3 METHODS

3.1 Connection Topology

In this study, two extended end-plate connections with four bolt rows were taken from Admuthe (2018). The two connections were for the same moment frame but were designed to have two different percentages of the plastic moment of the beam. Three moment frames were modeled in Admuthe (2018) with connection capacities of 50%, 60%, and 70% of the plastic moment of the beam to assess the performance under mainshock-aftershock sequences. These earthquake motions were determined using the earthquake suite provided, in part, by FEMA P-695 and complemented with other ground motions. The records were scaled to spectral accelerations between 0.1g and 4.0g at 0.1g intervals. The rotational outputs for the beam and column within the first-floor connections for each of the two frames were recorded in order to determine the relative rotations of the beam to the column. These values were then used as inputs for the component model to determine the forces in each bolt line and the moments undergone by the connection during each mainshock-aftershock sequence.

Only the 50% and 70% strength connections were modeled for the development of fragility curves. The end plate was 20mm thick and assumed to be made of A36 steel. The column was a W10x100 for the 70% strength connection and a W10x77 for the 50% strength, the beam for both strengths was a W21x50, and these were assumed to be A992 steel. The bolts were assumed to be A490N with a diameter of 25.4mm for the 70% and 20mm for the 50%. It was assumed that this connection was on the first story of a three story, three bay steel moment frame, shown in Figure 3-1.

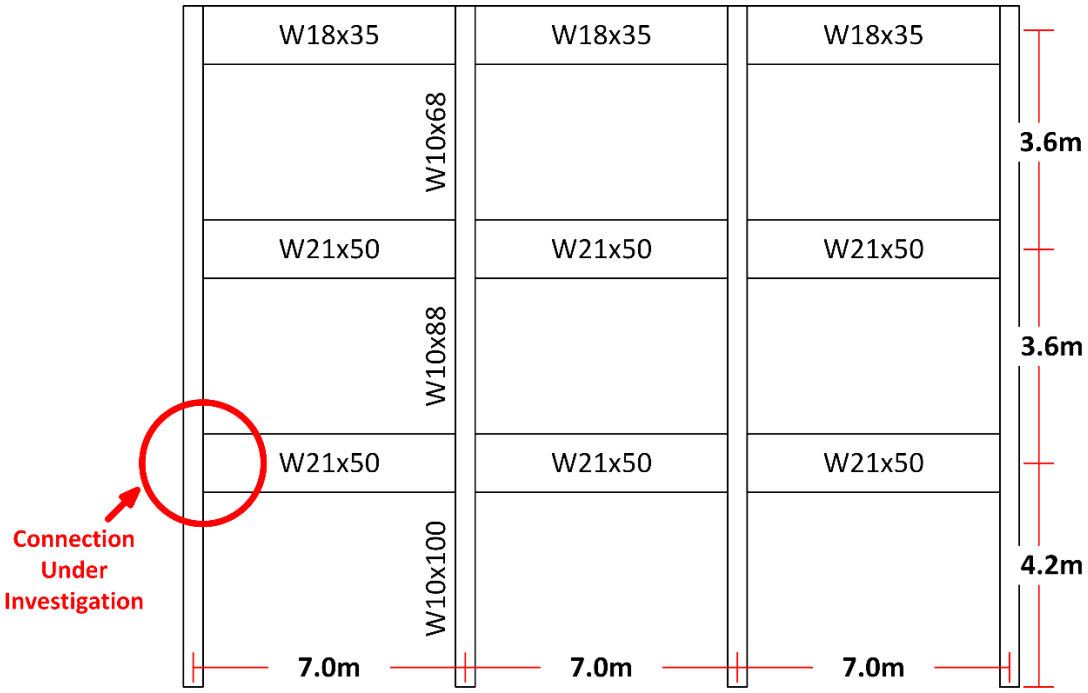

Figure 3-1. Elevation View of Semi-Rigid Structure with 70% capacity connections

3.2 Mechanical Model Component Characteristics

The unstiffened four-bolt extended end-plate connection was modeled using the Eurocode 3 component-based mechanical model where all components in the connection are integrated to obtain the full strength (CEN 2005). The active components within the connection included the column web subjected to axial tension and compression loads (cwa), the column flange in bending (cfb), the end-plate in bending (epb), the bolts in tension (bt), and the column web in shear (cws). These components can be seen in Figure 3-2. The components were aligned with each bolt row and the stiffnesses were calculated following Table 6.11 in EC3 Part 1.8 (CEN 2005). It should be noted that the column web in shear was only placed on the lower two bolt lines for the monotonic loading case. This is due to research conducted by Latour et al. (2011), which demonstrated that the column web in shear is only necessary to include on the compression side of the neutral axis.

Under cyclic loading, however, the contribution from the column web in shear was included for both sides of the neutral axis by considering the stiffness to be zero when in tension.

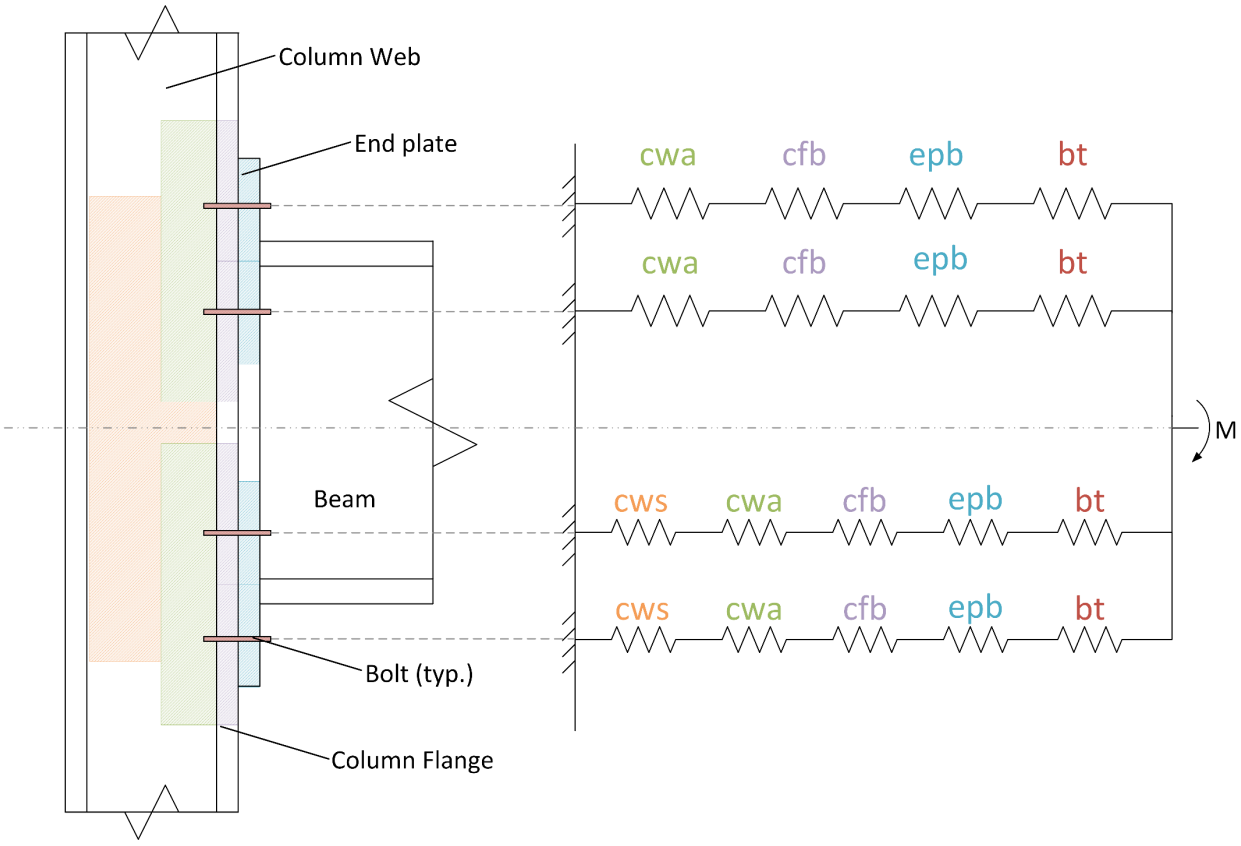

Figure 3-2. Component-based mechanical model

As seen in Figure 3-2, instead of the label ‘cwt’ or ‘cwc’, the label ‘cwa’ was used. This was due to the fact that in cyclic behavior, the bolt rows in tension and compression change. While all other components, except the cws, were assumed to have the same behavior in both tension and compression, the stiffness and strength were mirrored in the third quadrant. The column web loaded axially has different behavior in tension and compression according to the Eurocode, and these were taken into consideration within the actual component model programming.

Each of the spring components of the model followed a tri-linear behavior set forth by Girão Coelho (2004), which can be seen in Figure 3-3. The yield and ultimate strengths and

displacements for each spring were determined from Eurocode 3 Part 1.8 in the sections outlined in Table 3-1. The yield force and displacement (F_y and Δ_y) and the ultimate strength and corresponding displacement (F_u and Δ_u) are shown on Figure 3-3, and are the points at which the stiffness of the spring changes.

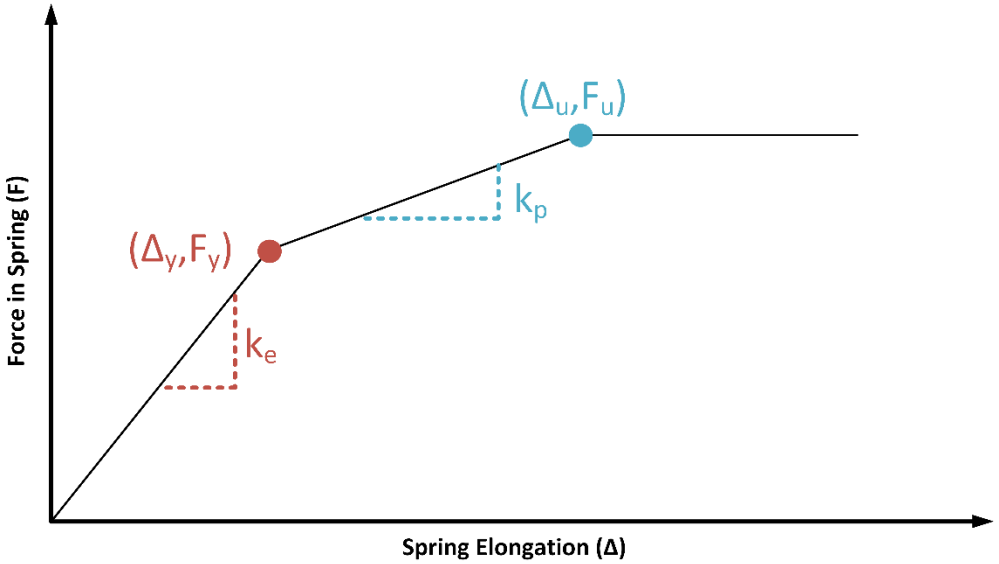

Figure 3-3. Spring Component Behavior

The elastic and plastic stiffnesses, k_e and k_p respectively, were determined using the equations found in EC 3 Table 6.11, displayed in Table 3-2 with variables defined in Table 3-3 (CEN 2005). In order to determine each spring stiffness, the modulus of elasticity and the strain hardening modulus had to be known. For the plastic stiffness, the strain hardening modulus was used in place of the modulus of elasticity, just as estimated in Girão Coelho (2004) and Jaspart (2000). Once these were known, the yield force and ultimate force were found using the appropriate sections of the Eurocode, laid out below in Table 3-1.

Table 3-1. Eurocode 3 Sections for Determining Yield and Ultimate Forces for Component Springs

Component	Component Abbrev.	EC 3 Part 1.8 Section
Unstiffened column web panel in shear	cws	Section 6.2.6.1
Unstiffened column web in compression	cwa	Section 6.2.6.2
Unstiffened column web in tension	cwa	Section 6.2.6.3
Column flange in bending	cfb	Section 6.2.6.4
End-plate in bending	epb	Section 6.2.6.5
Bolt row in tension	bt	Table 3.4

Table 3-2. Eurocode 3 Component Stiffness Equations

Component	Component Abbrev.	Spring stiffness Coefficient
Unstiffened column web panel in shear	cws	$k_{cws} = \frac{0.38 A_{vc} E}{\beta z}$
Unstiffened column web in compression	cwa	$k_{cwc} = \frac{0.7 b_{eff,c,wc} t_{wc} E}{d_c}$
Unstiffened column web in tension	cwa	$k_{cwc} = \frac{0.7 b_{eff,t,wc} t_{wc} E}{d_c}$
Column flange in bending	cfb	$k_{cfb} = \frac{0.9 l_{eff} {t_{fc}}^3 E}{m^3}$
End-plate in bending	epb	$k_{epb} = \frac{0.9 l_{eff} {t_p}^3 E}{m^3}$
Bolt row in tension	bt	$k_{bt} = \frac{1.6 A_s E}{L_b}$

Table 3-3. Definitions of variables in Table 3-2

Variable	Definition
A_{vc}	Area of the column subjected to shear
A_s	Area of the bolts in a bolt row
$b_{eff,c,wc}$	Effective width of the column web in compression
$b_{eff,t,wc}$	Effective width of the column web in tension
d_c	Clear depth of the column web
E	Modulus of elasticity of the material
L_b	Bolt elongation length
l_{eff}	Effective length for an unstiffened column flange for the given bolt row
m	Distance from the inner bolt to the beginning of the chamfer of the column web
t_{fc}	Thickness of the column flange
t_p	Thickness of the end plate
t_{wc}	Thickness of the column web
z	Lever arm of the moment, taken as the distance between the center of compression and the center of the beam flange in tension
β	Transformation parameter defined in section 5.3(7) of EC3 Part 1.8

3.3 Validation of Mechanical Model

In order to ensure that the model was running as expected, it was compared to two separate studies involving extended end-plate connections where the experimental results and the connection geometries were available. As component-based mechanical models are generally only

used for monotonic loading, the model was first compared to results given in Del Savio et al. (2009). The MATLAB model developed for the study showed acceptable agreement between the experimental and model data under monotonic loading, as seen in Figure 3-4. It should be noted that the Eurocode models are conservative, which is acceptable in design as a level of conservatism is desired.

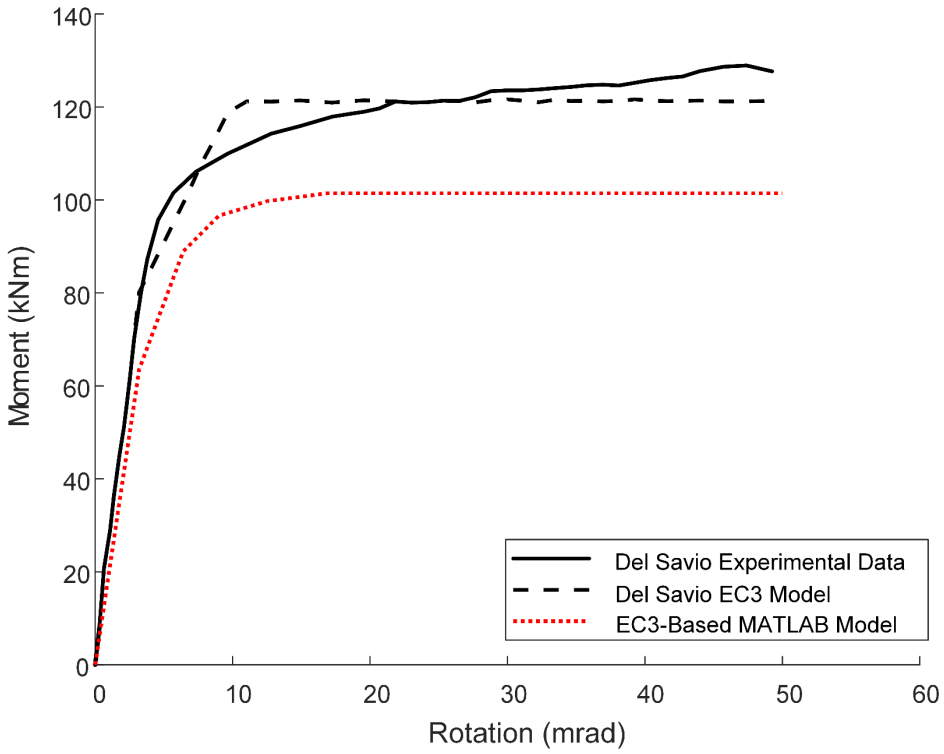

Figure 3-4. Monotonic Loading Comparison of EC3-based MATLAB Model to Del Savio 2009 Data

Once the model was validated against another similar model, the application of cyclic loading was also compared to data from Ghobarah et al. (1990) to determine whether the cyclic behavior of the model was acceptable. As can be seen in Figure 3-5, the MATLAB model has a conservative approximation of the behavior but has an acceptable agreement between the initial stiffnesses. It can be seen in Figure 3-6 that the backbone curves between the experimental data

from Ghobarah et al. (1990) and the MATLAB model have a similar relationship to that of the monotonic loading scenario shown in Figure 3-4, which is a conservative approximation of the experimental strength. These tests were considered sufficient for validation of the model as it performed as expected when compared to the literature available.

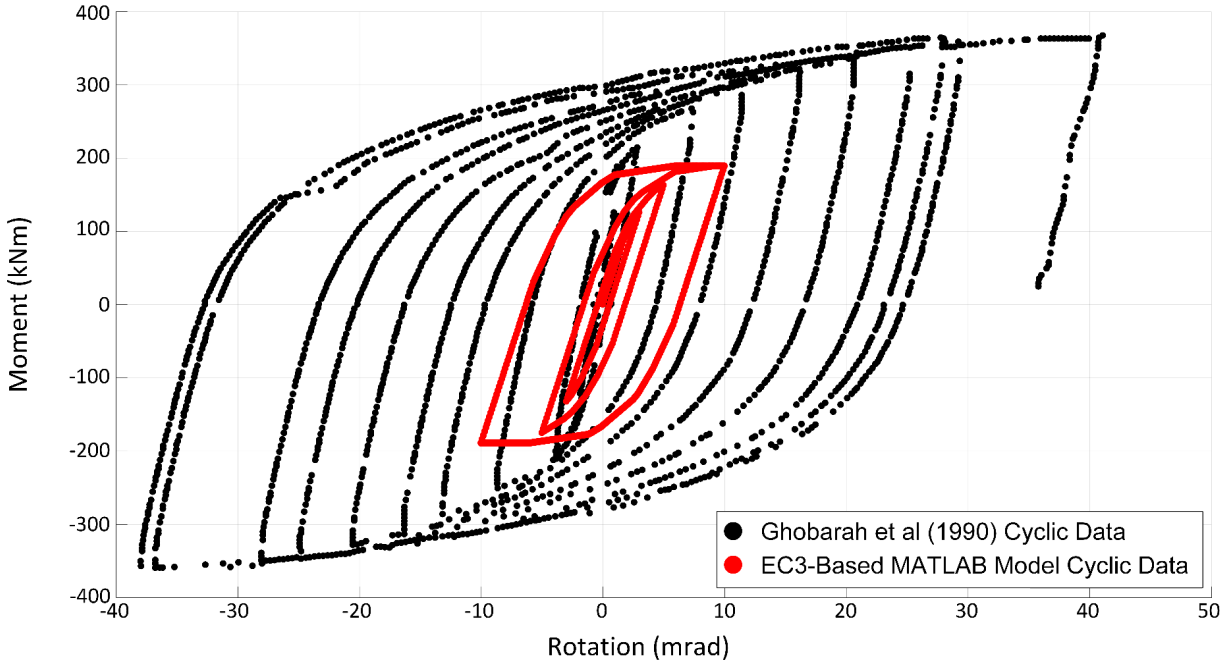

Figure 3-5. Comparison of Cyclic Loading for EC3-based MATLAB Model to Experiment from Ghobarah et al (1990)

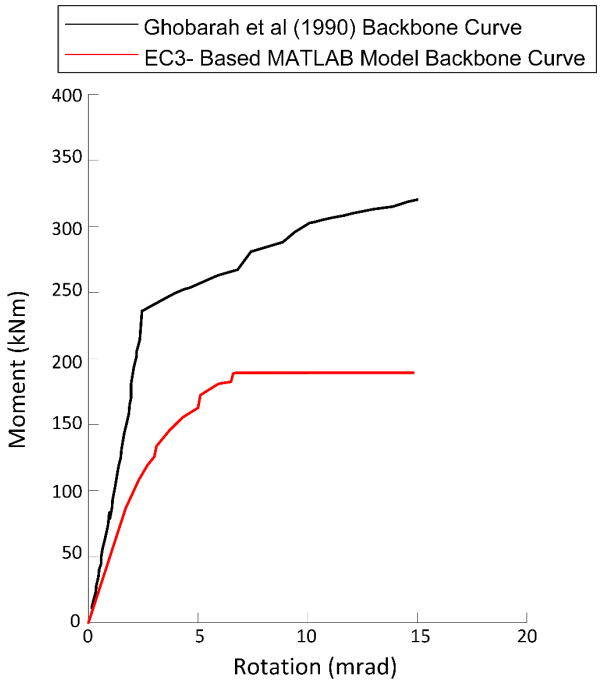

Figure 3-6. Comparison of Backbone Curves from Cyclic Loading for EC3-based MATLAB Model to Experiment from Ghobarah et al (1990)

3.4 Development of the Understrength Factor

During model validation, it was observed that the Eurocode component-based models underestimated the actual strength of the connection, as seen in Figure 3-4 and Figure 3-5. This behavior was further confirmed through extensive evaluation of the literature as shown Figure 3-7.

In design, this gives an inherent conservative approximation to the strength of the connection, which is often desirable. However, for the purpose of research, a more accurate representation of the joint behavior is necessary. In order to account for this difference between experimental and estimated behavior, an understrength factor was developed using data from previous studies with both experimental data and EC3 component models for four-bolt extended end-plate connections from Abidelah et al. (2012), Baei et al. (2012), Borges (2003), Girão Coelho (2004), Prinz et al. (2014), and Shaker and Abd Elrahman (2014).

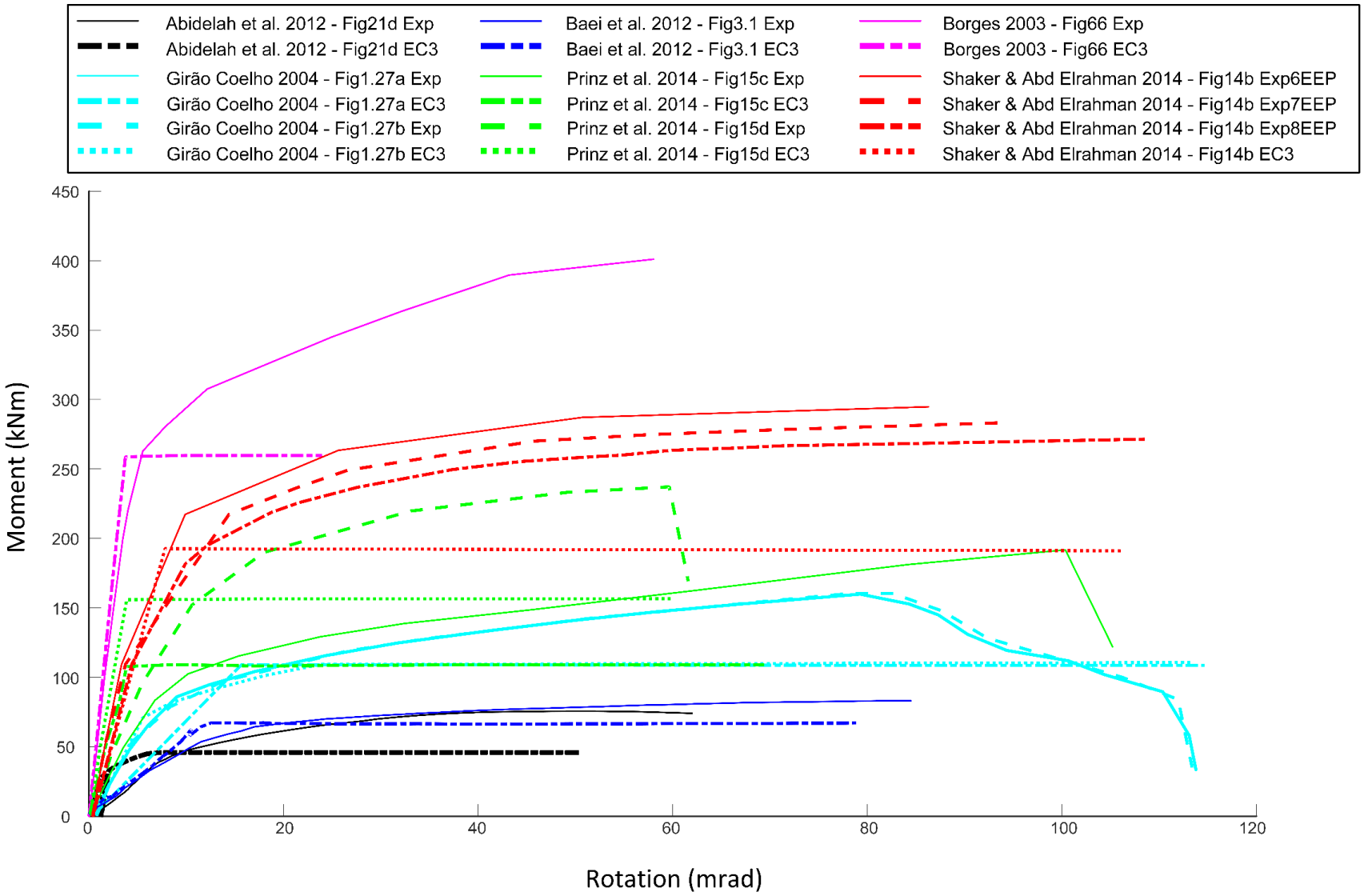

Figure 3-7. Survey Comparison of the Disparity in EC3-based Models and Experimental Strength for Extended End-Plate Connections

To calculate the understrength factor, the value of the rotation of the experimental curve was determined for the maximum moment estimated by the EC3 model, indicated by the intersection of the EC 3 maximum moment with the experimental curve shown in Figure 3-8.

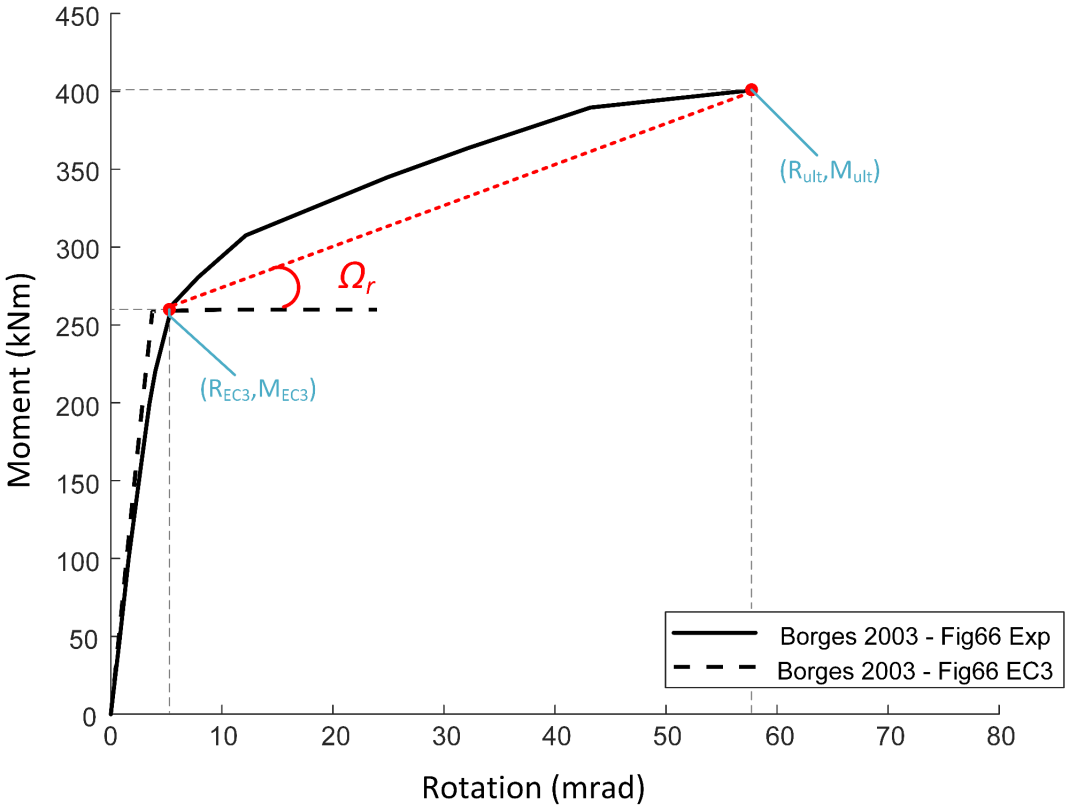

Figure 3-8. Definition of Understrength Factor using Experimental and EC3 Model Results

The maximum rotation and moment were also determined for the experimental curve and a secant line was drawn between the two points to estimate the angle between the two lines. This value, calculated as shown in Equation 3-1, was used as the understrength factor and applied to the EC3 model to better estimate the actual moment of the connection.

$$\Omega_r = \tan^{-1}\left(\frac{M_{ult} - M_{EC3}}{R_{ult} - R_{MEC3}}\right) \qquad \textit{Equation 3-1}$$

where Ω_r is the understrength factor

M_{ult} = the ultimate strength of the experimental curve

R_{ult} = the rotation corresponding to M_{ult}

M_{EC3} = the ultimate strength estimated by Eurocode 3

R_{MEC3} = the experimental rotation corresponding to M_{EC3}

Once the understrength factor was determined, it was applied to the EC calculated model after the point at which the moment became constant. This was realized by calculating a new moment based upon the understrength factor determined for the curve.

$$M_{cor} = M_{EC3} + (R - R_{const}) * \tan \Omega_r \qquad \textit{Equation 3-2}$$

where M_{cor} = the moment after understrength corrections

R = the rotation corresponding to M_{cor}

M_{EC3} = the ultimate strength estimated by Eurocode 3

R_{const} = the rotation corresponding to the first occurrence of M_{EC3}

Ω_r = the understrength factor

Once the understrength factor had been developed, the factors for each of the studies shown in Figure 3-7 were calculated and compared to a normal distribution to determine whether the understrength factor was a valid assumption. The Ω_r was calculated for all eleven cases, and a mean of 0.91 and a standard deviation of 0.17 were determined. The understrength values were then rank-ordered using the standard sample rank-ordering process to determine the cumulative probability of occurrence. The mean and standard deviation were the used to determine the cumulative probability of occurrence of the same understrength factors. As can be seen in Figure 3-9, the rank-order and normal distribution give very similar results. The coefficient of

determination between the rank-ordered data and the normally distributed regression was a value of 0.966, which was deemed acceptable to assume that the understrength factor follows a normal distribution.

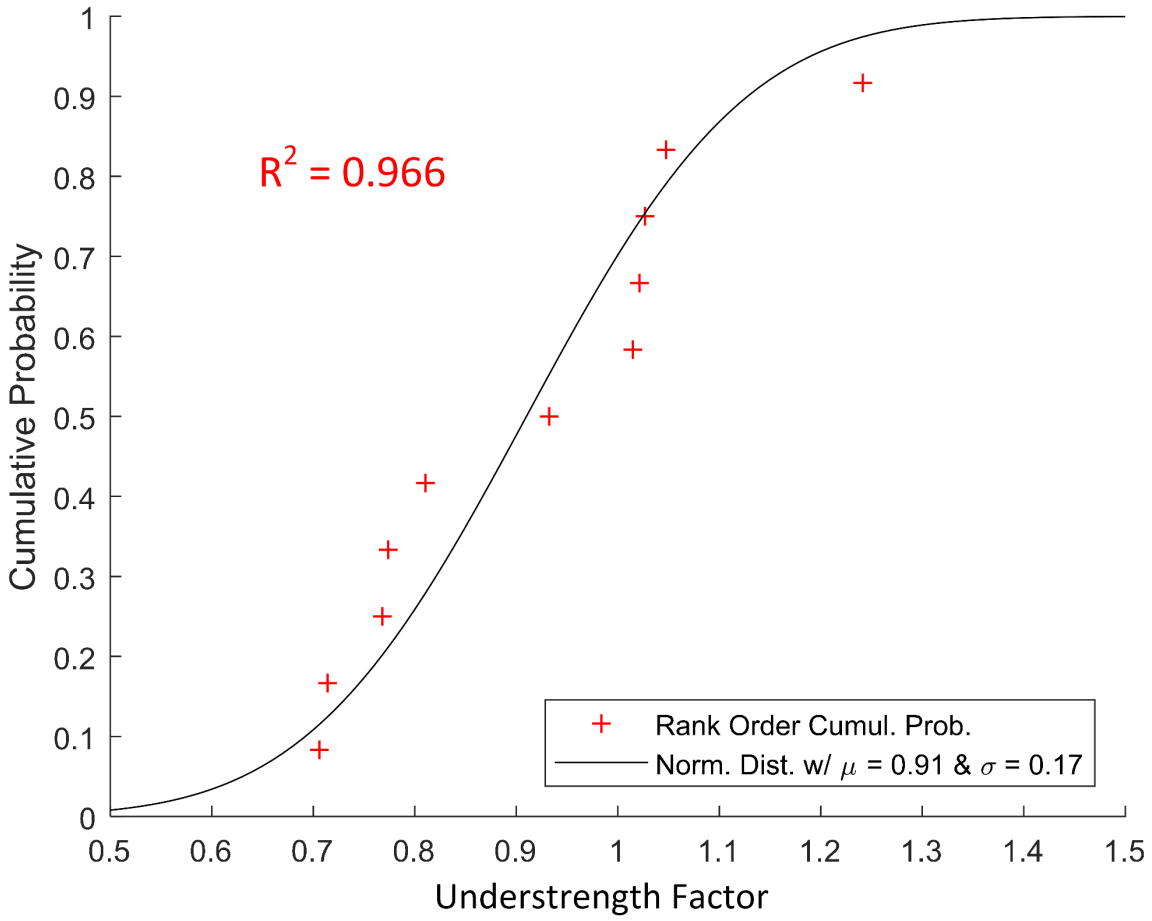

Figure 3-9. Comparison of rank-order to normal distribution of the understrength factor

Once the understrength factor was developed, it was applied to the original validation against Del Savio et al. (2009). As seen in Figure 3-10, the model that includes the understrength factor more accurately represents the experimental behavior of the connection. It should also be noted, as shown in Figure 3-11, that during cyclic loading of the model, the understrength factor

affects the plastic stiffness of the model and the moment associated with the rotation but does not affect the initial elastic stiffness of the model.

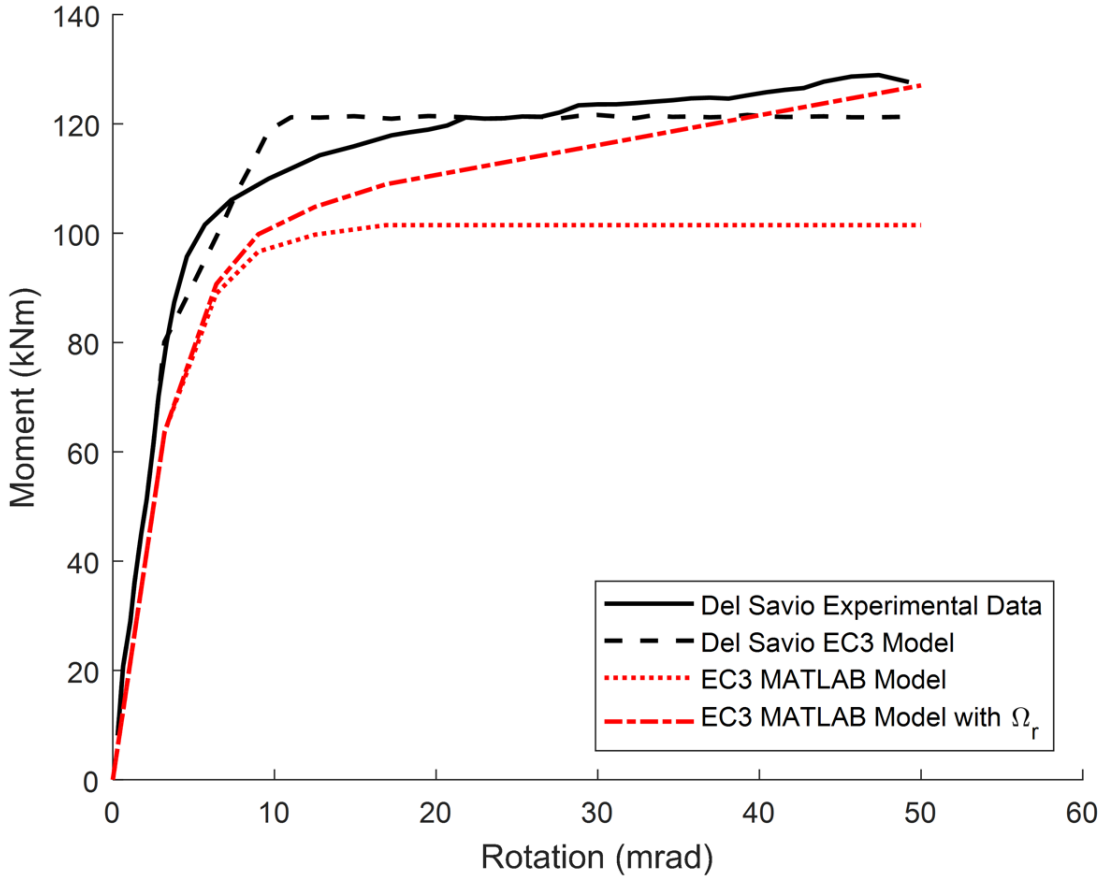

Figure 3-10. Comparison of unmodified EC3 model to EC3 model with understrength factor

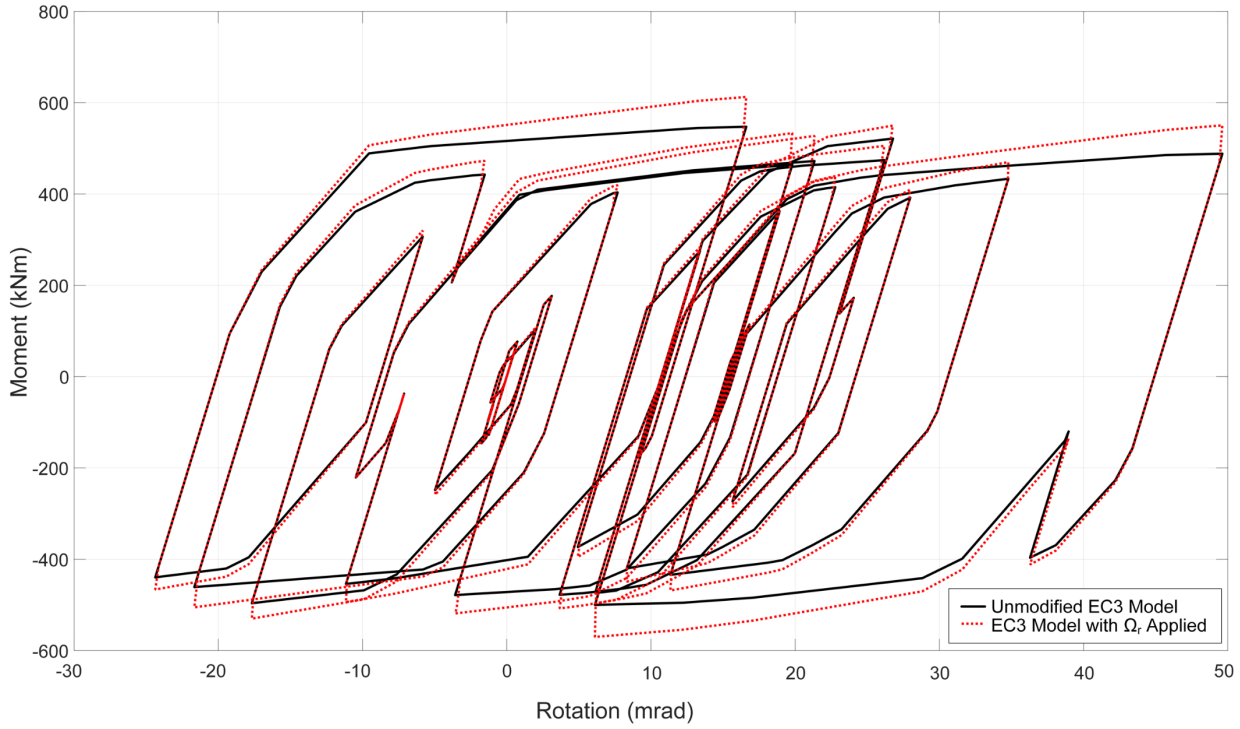

Figure 3-11. Comparison of cyclic loading for unmodified EC3 model to EC3 model with understrength factor

3.5 Development of Fragility Curves

Fragility functions are created to demonstrate the probability of exceeding a given failure criterion when a particular event occurs. For the purpose of this study, the event under consideration was the mainshock-aftershock sequence between a spectral acceleration of 0.1g and 4.0g.

During design of extended end-plate connections, there are fourteen separate limit states to consider, as stated by the AISC seismic design guide for end-plate connections, which are outlined in Table 3-4 (Murray and Sumner 2003). The connections were evaluated for failure based upon some of the limit states discussed in Table 3-4.

Table 3-4. Limit States for Extended End-Plate Connections (Murray and Sumner 2003)

Number	Limit State
1.	Flexural yielding of the end-plate material near the tension flange bolts.
2.	Shear yielding of the end-plate material.
3.	Shear rupture of the unstiffened end plate through the outside line of bolt holes.
4.	Bolt rupture in tension.
5.	Bolt shear failure at the interface between the end plate and the column flange.
6.	Bearing failure of the end plate or column flange at the bolts.
7.	Rupture of the welds in tension between the beam flange and end plate or the beam web and end plate.
8.	Shear yielding of the weld or beam web base metal at the end plate weld.
9.	Column web yielding opposite one of the beam flanges.
10.	Column web crippling opposite the compression flange of the beam.
11.	Column web buckling opposite the compression flange of the beam.
12.	Flexural yielding of the column flange in the vicinity of the tension bolts.
13.	Failure of the column transverse stiffener due to yielding, local buckling, or weld failure.
14.	Column panel zone failure due to shear yielding or web plate buckling.

These earthquake scenarios, which were represented using rotations obtained from Admuthe (2018) that are applied to the EC3 connection model in this study, were evaluated for approximately 650 different variations in connection material properties to determine the probability of failure of the connection. The material properties of the connection were varied for each iteration according to the mean and coefficient of variation presented by Galambos (1981)

for the respective material property, shown in Table 3-5. The understrength factor was also varied normally for each iteration, following the mean and standard deviation shown in Figure 3-9.

Table 3-5. Statistical Variation of Material Properties (Galambos 1981)

Property	Mean	Coefficient of Variation
Yield stress (flanges)	1.05Fy	0.10
Yield stress (webs, plates)	1.10 Fy	0.11
Modulus of Elasticity	E	0.06
Tensile Strength	1.10Fu	0.11
Tensile Strength of H.S.S. bolts, A490	1.07Fu	0.02

While some limit states in Table 3-4 could be addressed through the use of the component-based model, others could not be addressed. Limit states 2, 3, and 5 all dealt with the shear forces acting perpendicular to the line of the springs, which were not calculated due to the axial nature of the springs. In order to address these limit states, additional springs running in parallel with the shear forces would need to be added and would increase the computational time. The AISC manual notes that limit state 2 is not usually observed, and so adjustments were not made to include additional shear springs (Murray and Sumner 2003).

Limit states 7 and 8 required the beam and welds within the connection to be modeled. Following EC3 Table 6.11 notes 3 and 4, the beam and weld stiffnesses were not used to determine the rotational stiffness and were not included within the mechanical model utilized.

Limit states 10 and 11 required the shear force at the location of the plastic hinge in order to calculate the moment at the face of the column. The shear force at the plastic hinge was not

provided with the joint rotations from the semi-rigid frame and so could not be considered for calculation of these limit states.

Limit state 13 only applied to stiffened columns and was therefore not applicable to the current model.

Thus, limit states 1, 4, 6, 9, 12, and 14 were checked against the model outputs. Additionally, the acceptance criteria for life safety, collapse prevention, and strength degradation based upon rotations outlined in Aksoylar et al. (2011) were also compared to the rotations of each connection, shown in Table 3-6.

Table 3-6. Acceptance Criteria for Connection Rotation (Aksoylar et al. 2011)

Acceptance Criteria	Rotation (rad)
Life Safety	0.028
Collapse Prevention	0.035
Strength Degradation	0.042

The bolt rupture in tension was directly comparable between the ultimate strength of the bolts and the forces in each bolt line. Values above the ultimate strength of the bolt were considered to have failed. The number of bolt lines that failed for each of the spectral accelerations was also calculated based upon the number of bolt rows which exceeded the ultimate strength of the bolts within the same simulation.

Column web yielding was directly comparable to the model outputs following the ultimate strength of the column web in tension and/or compression. The maximum tensile and compressive loads within the cwa spring were compared to the yield strengths of the column and values exceeding the ultimate strengths were considered as a failure for computation of the fragility

curves. Column web in shear was also directly comparable to the model outputs, and the maximum shear load within the cws spring was compared to the yield strength of the web in shear. As with column web yielding, values above the shear yield strength were considered to have failed.

The bearing failure of the end plate or column flange was also directly comparable to the forces within the component and were compared to the yield strengths of the materials. These followed the same procedure as the column web.

For the flexural failure comparisons, equations for the allowable moments within the components were followed from the AISC design guide. The moment calculated with the model was compared to the moment as calculated in Equation 3-3.

$$M_{np} = \frac{\Phi_b F_{yp} Y_p {t_p}^2}{1.11\Phi} \qquad \textit{Equation 3-3}$$

where M_{np} = the maximum allowable moment for the connection

$\Phi_b = 0.9$

$\Phi = 0.75$

F_{yp} = the yield strength of the end plate

t_p = the thickness of the end plate

Y_p = the end plate yield line mechanism parameter (defined in AISC design guide tables 3.1,3.2, or 3.3)

For the column flange, a similar equation was used, shown in Equation 3-4.

$$M_{np} = \frac{\Phi_b F_{yc} Y_c {t_{fc}}^2}{1.11\Phi} \qquad \textit{Equation 3-4}$$

where F_{yc} = the yield strength of the column

t_{fc} = the thickness of the column flange

Y_c = the unstiffened column flange yield line mechanism parameter (defined in AISC design guide tables 3.4 or 3.5)

Once the values were determined for each limit state, the maximum tensile or compressive force or the maximum moment was compared to the limiting value. If the value was exceeded, it was deemed to have failed for that iteration. This was repeated at each spectral acceleration between 0.1g and 4.0g approximately 650 times in order to create a large sample for determination of the probability of failure independent of the material properties.

These probabilities were then fitted to the standard accepted fragility function defined in Porter (2018), which is shown in Equation 3-5.

$$F_d(x) = \Phi\left(\frac{\ln\left(\frac{x}{\theta_d}\right)}{\beta_d}\right) \qquad \textit{Equation 3-5}$$

where $F_d(x)$ = the fragility function for a damage state, d, evaluated at a particular value of the uncertain excitation, *x*

$\Phi(s)$ = the standard normal cumulative distribution function evaluated at *s*

x = a particular value of the uncertain excitation under consideration

θ_d = median capacity of the connection to resist the damage state, d

β_d = standard deviation of the natural logarithm of the capacity of the connection to resist the damage state, d

Once the fragility functions for the limit states were developed, it was possible to compare the fragility functions for the mainshock-aftershock sequences considering the entire sequence, as well as the mainshock and aftershock separately.

4 RESULTS AND DISCUSSION

Once the results of the Monte Carlo simulations of the connection models were processed, the following limit states were checked to determine the probability of failure and the development of the fragility functions:

1. Tensile force in the bolts exceeding the ultimate strength
2. Shear force in the column web exceeding the shear strength
3. Tensile/compressive force in the column web exceeding the axial strength
4. Moment in the column flange exceeding the bearing strength
5. Tensile/compressive force in the end plate exceeding the axial strength
6. Moment in the end plate exceeding the bearing strength
7. Rotation of the beam exceeding the life safety, collapse prevention, and strength degradation limits

As noted previously, other limit states for the end plate connections exist (listed in Table 3-4). They were not, however, checked, and therefore not discussed in this chapter since the mechanistic models are incapable of capturing these limit states. In addition, for both the 50% and 70% strength connections, for the range of spectral accelerations simulated, the model outputs never exceeded the bearing strengths of the end plate or column flange or the axial strengths of the end plate or column web. As such, while these limit states were considered during analysis, they are not discussed herein as the fragility functions equate to zero for the given range of spectral accelerations.

The 50% and 70% connections were both modelled using the rotations obtained from the frame-level analysis in Admuthe (2018) for the mainshock-aftershock sequence, and the results

were then separated to produce three different data sets: failure occurring during just the mainshock ground motions, failure occurring during just the aftershock ground motions, and failure occurring in either or both the mainshock and aftershock motions.

4.1 Tensile Force in the Bolts

According to Murray and Sumner (2003), the primary limit state to be considered in design of extended end-plate connections is the failure of the bolts in tension. As such, the number of bolts where the tensile force exceeded the strength of the bolt was recorded for each of the spectral accelerations and simulations. With four bolt rows, each with two bolts, the fragility functions were broken down into the probability of two or more bolts, four or more bolts, six or more bolts, and all eight bolts failing.

As seen in Figure 4-1 a through d, which shows the fragility functions for an increasing number of bolt failures for the 50% connection, the failure probabilities of an increasing number of bolts decreases, with the probability of all eight bolts failing having the smallest probability, as expected, while the probability of two or more bolts failing was the largest. It can also be seen in Figure 4-1, that for all cases of bolt failure, the mainshock-aftershock fragility function is most shifted to the left, also as expected. In all cases, the aftershock ground motions produced a higher probability of failure than the mainshock, which indicates that the connection is more likely to fail during the aftershock. This was anticipated as there are residual forces and displacements from the mainshock event that is carried over into the aftershock. Additionally, the difference between the probabilities of the mainshock event and the aftershock event decreases with an increase in the number of failed bolts.

Some of the fitted fragility functions do not appear to be asymptotically approaching a failure probability of 1, as seen in Figure 4-1 c and d. This is attributed to the fact that all of the model outputs had relatively low failure probabilities. The curve fitting would change with a larger range of spectral accelerations; however, since Figure 4-1 a and b show the anticipated shape of the fragility function, and any number of bolts failing is deemed a failure of the entire connection, a larger range of spectral accelerations was not investigated.

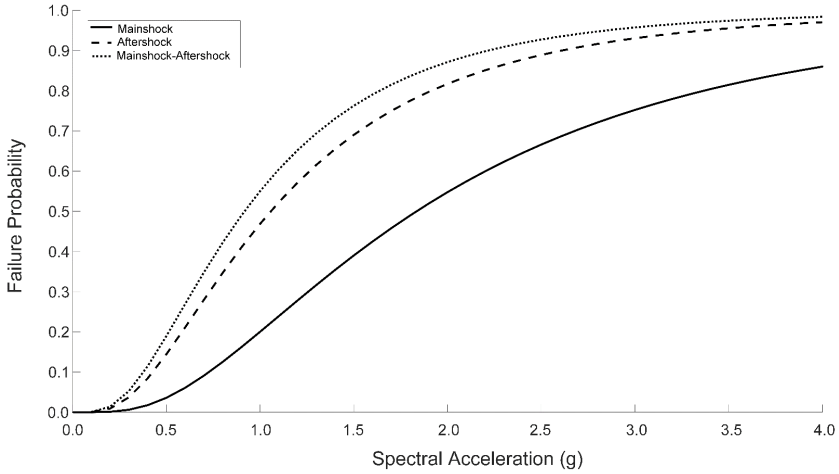

a) Two or more bolts fail

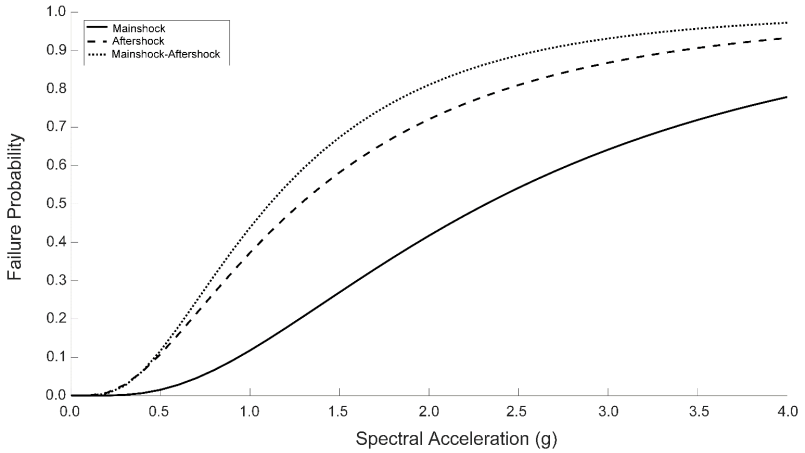

b) Four or more bolts fail

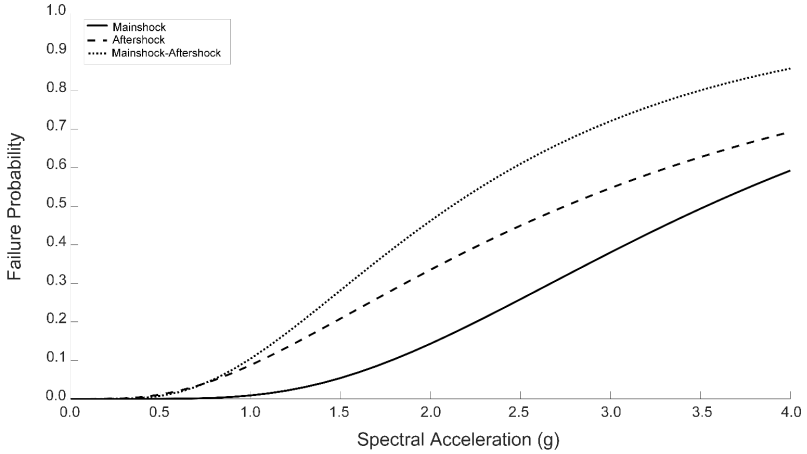

c) Six or more bolts fail

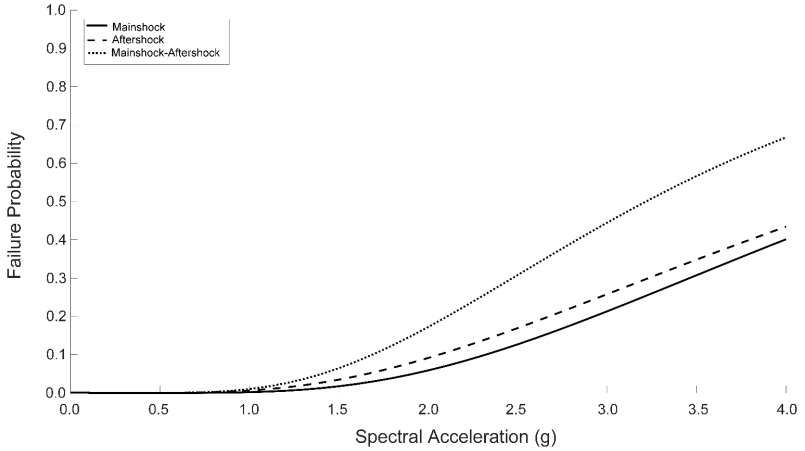

d) All eight bolts fail

Figure 4-1. Fragility functions for bolts in tension of the 50% connection

The 70% connection demonstrated slightly different behavior, with the mainshock fragility functions, shown in Figure 4-2 a through d, having a higher probability of failure than the aftershock for most of the spectral accelerations under investigation. For two or more bolts and four or more bolts failing in tension, aftershock has a higher probability of failure until a spectral acceleration of approximately 1.0g and 1.5g respectively, at which point the failure probability during the mainshock event exceeds that during the aftershock event. For the six or more bolts failing, the failure probability during the mainshock event appears to be higher until approximately 3.0g, when the failure probability during the aftershock event exceeds that during the mainshock. The eight bolts failing appears to have a similar behavior but cannot be fully observed as the intersection point occurs at 4.0g. This behavior implies that the connection is more likely to fail during the mainshock event than during the aftershock for the range of spectral accelerations under investigation.

As projected, the mainshock-aftershock sequence fragility functions produced the highest failure probabilities in all cases. The fragility functions for the six or more bolts and the eight bolts, seen in Figure 4-2 c and d, have the same linear shape as eight bolts failing for the 50% connection, and this is attributed to the same collection of low failure probabilities.

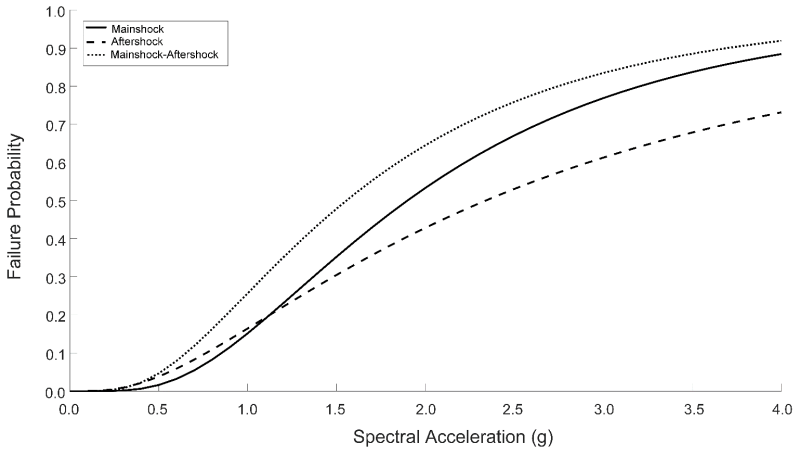

a) Two or more bolts fail

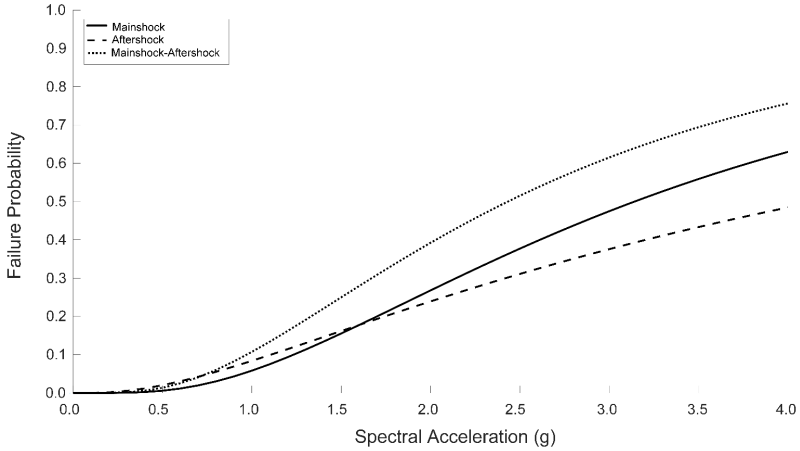

b) Four or more bolts fail

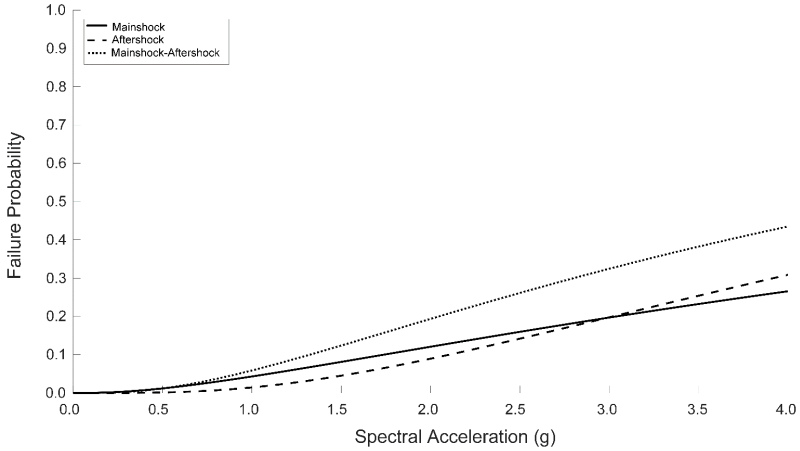

c) Six or more bolts fail

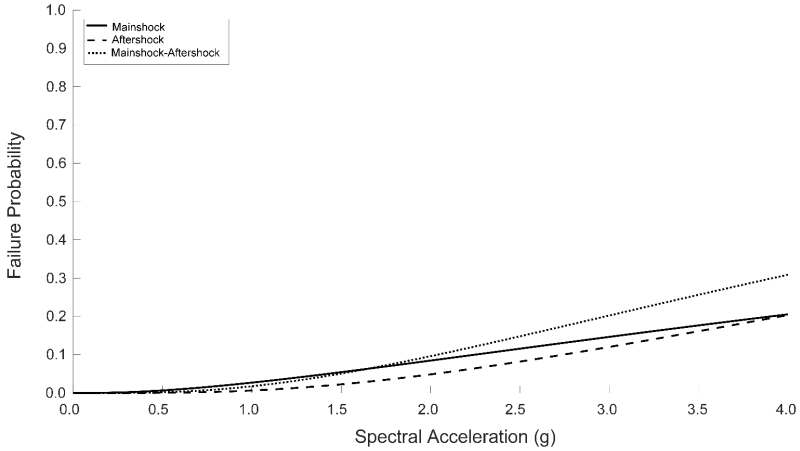

d) All eight bolts fail

Figure 4-2. Fragility functions for bolts in tension of the 70% connection

When comparing the failure probabilities of the 50% and 70% connections, as seen in Figure 4-3, for all cases of bolt failure, the 50% connection has a higher probability of failure. This is to be expected as the bolts from the 70% connection have a diameter of 25.4mm while the 50% connection bolts have a 20mm diameter. The additional nominal area of the bolts on the 70% connection allows for a larger force before failure occurs, thus decreasing the probability of failure under the ground motions.

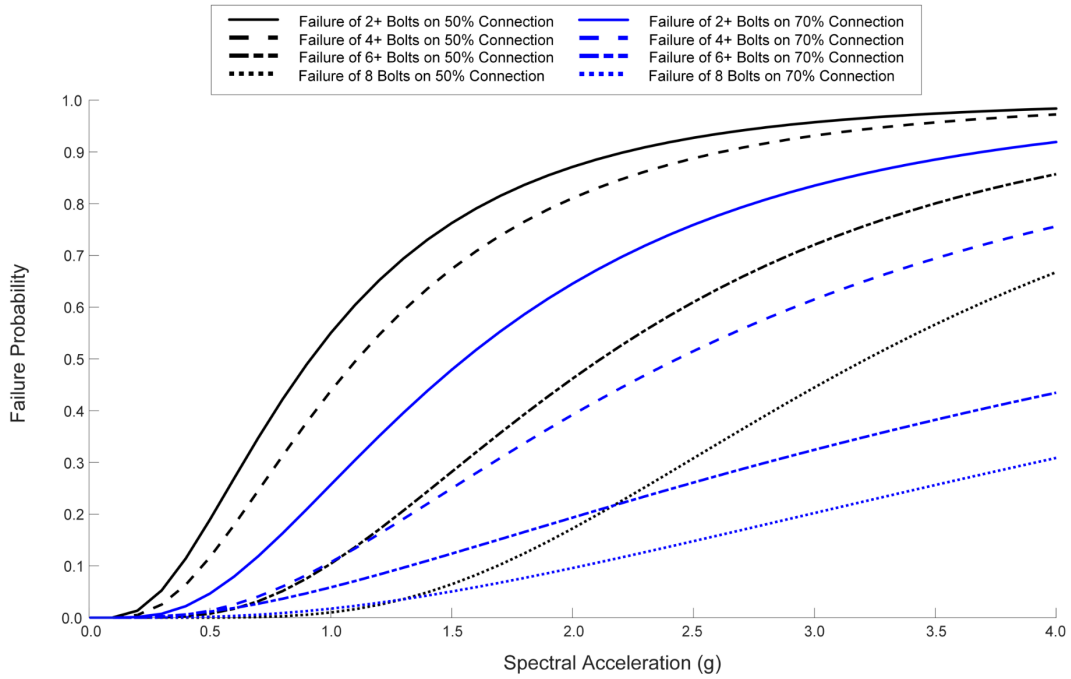

Figure 4-3. Fragility functions for bolts in tension during the mainshock-aftershock sequence

4.2 Shear Force in the Column Web

For the modelled range of spectral accelerations, the probability of failure by the column web in shear fell below 0.6 for the 50% connection. As seen in Figure 4-4, the majority of the failures occurred during the aftershock ground motions, as opposed to during the mainshock, which had less than a 0.1 probability of failure during a mainshock corresponding to the spectral acceleration of 4.0g. It should be noted that the mainshock-aftershock fragility function should be

equal to or shifted to the left of both the mainshock and aftershock functions, which did not occur for this curve fitting; however, as seen in Figure 4-5, all of the collected data points for the mainshock-aftershock sequence are equal to or exceed the other two data sets. As such, the range in which the aftershock fragility function exceeds the mainshock-aftershock function is attributed to the nature of curve fitting and the low failure probabilities. These functions also do not appear to asymptotically approach 1, which is again attributed to the low probabilities for the range of spectral accelerations investigated. Should a larger range of spectral accelerations be considered, it is believed that the additional data would produce fragility functions closer in shape to those that were anticipated.

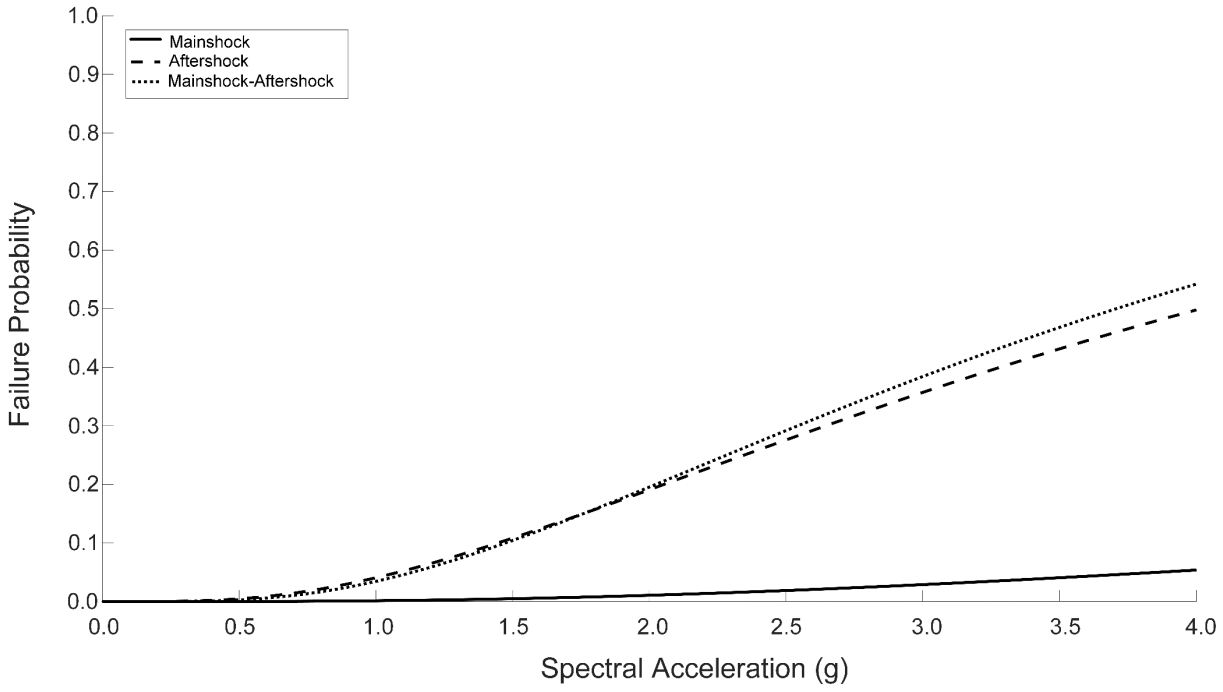

Figure 4-4. Fragility functions for the column web failing in shear of the 50% connection

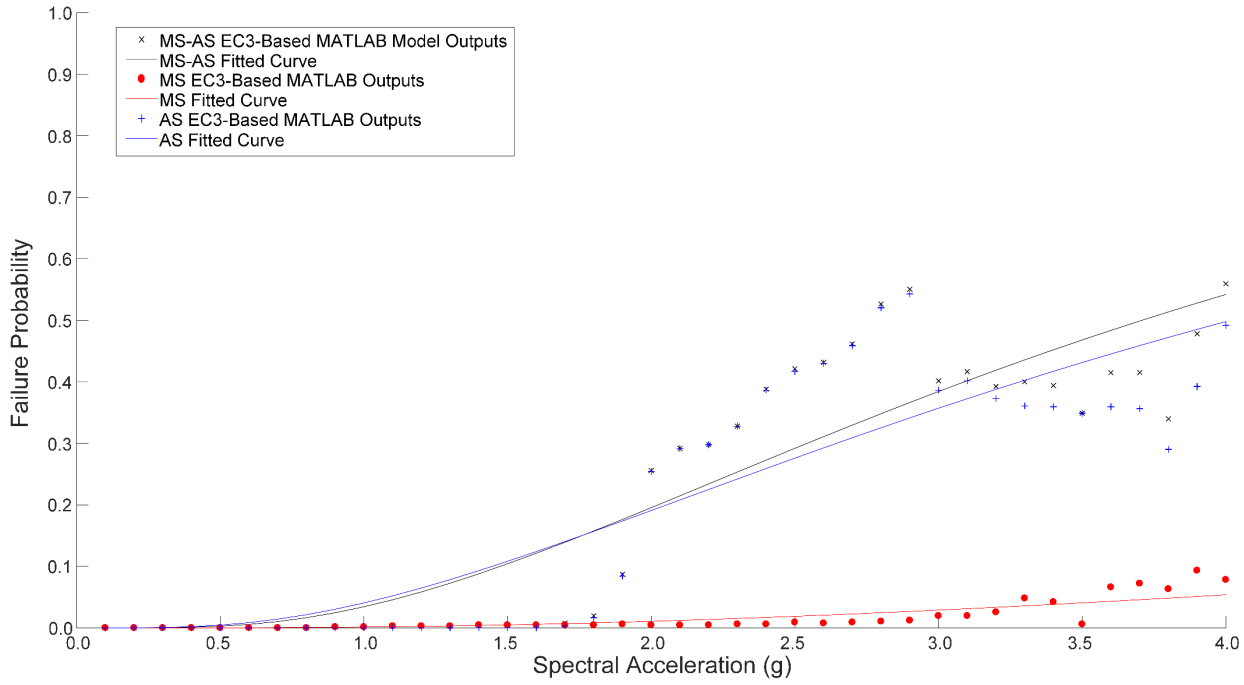

Figure 4-5. Fragility functions for the column web failing in shear of the 50% connection with data points shown

Similar to the 50% connection, the 70% connection fragility functions do not appear to asymptotically approach 1, but rather have a more linear appearance to them, as seen in Figure 4-6. Unlike the 50% connection, the mainshock-aftershock sequence does bound both the mainshock and aftershock ground motion fragilities. It should be noted that adding the failure probabilities of the mainshock function and the aftershock function may exceed that of the corresponding mainshock-aftershock sequence as there were multiple cases in which the connection failed both during the mainshock and the aftershock ground motions but was only counted as failing once for the mainshock-aftershock sequence.

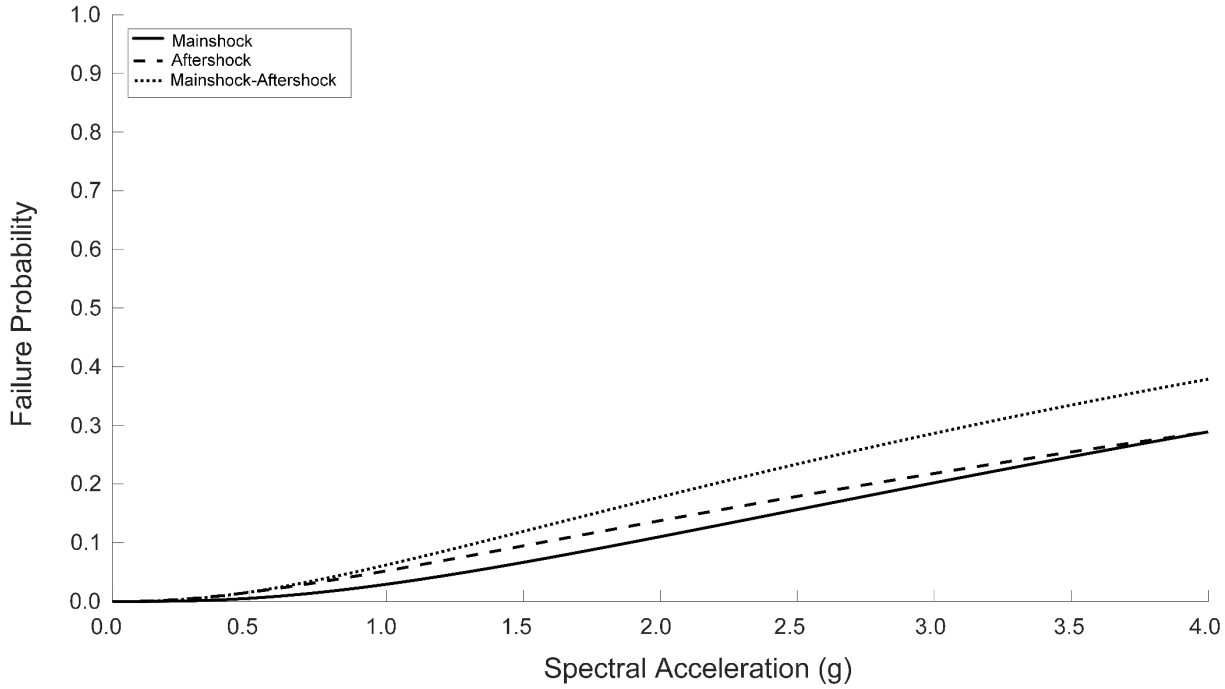

Figure 4-6. Fragility functions for the column web failing in shear of the 70% connection

As predicted, the 50% connection has a larger probability of failure of the column web in shear than the 70% connection, seen in Figure 4-7. This is to be expected as the column size for the 70% connection is W10x100 column while for the 50% connection it is W10x77. The additional cross-sectional area of the W10x100 corresponds to a larger capacity in shear, hence the lower probability of failure, as observed from the model outputs.

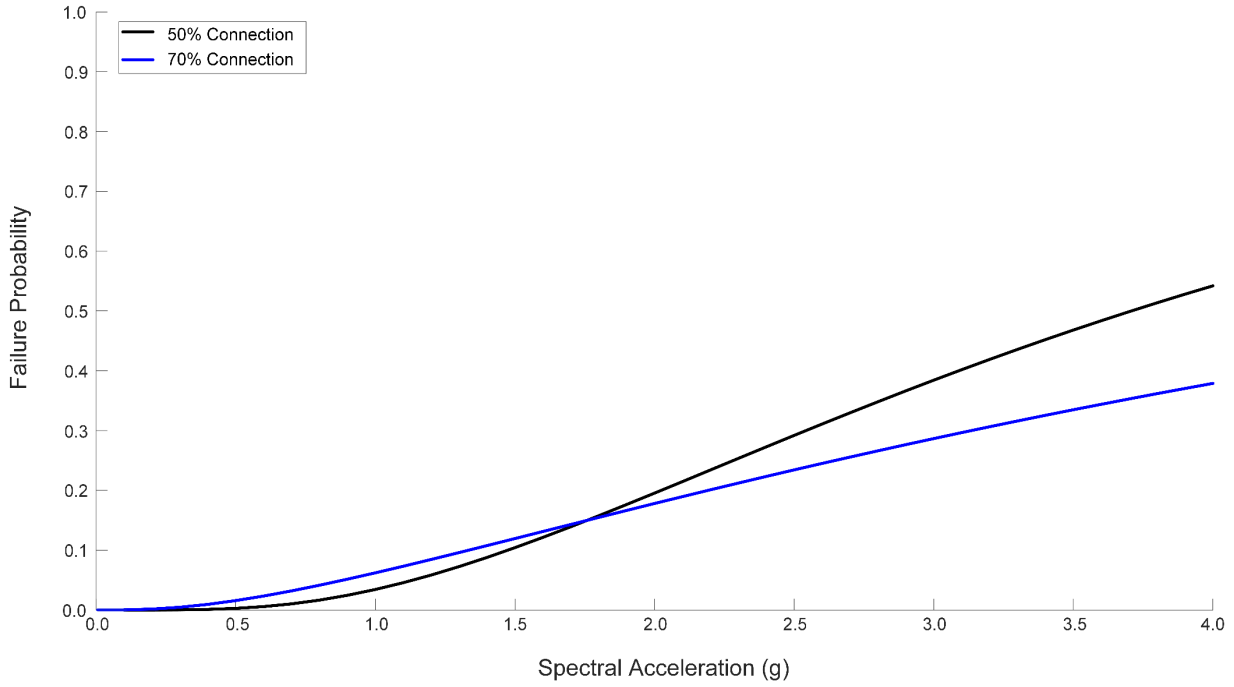

Figure 4-7. Fragility functions for the column web failing in shear during the mainshock-aftershock sequence

4.3 Rotation of the Beam

Three separate rotation limit states were compared to the relative rotations of the beam to the column of the extended end-plate connections to create fragility curves. The three limit states were life safety (0.028 radians), collapse prevention (0.035 radians), and strength degradation (0.042) (Aksoylar et al. 2011). The relative rotations were the input values for the mechanical model and were calculated based upon the absolute rotations of the column and beam from Admuthe (2018) for the 70% and 50% connections.

For each of the rotation limit states, fragility functions were created for the mainshock, aftershock, and mainshock-aftershock sequence. As seen in Figure 4-8, for the 50% connection, the mainshock-aftershock sequence gives the largest failure probability at a given spectral acceleration, as anticipated. However, the mainshock event and aftershock event fragility functions

intersect at a spectral acceleration of approximately 2.5g. For lower spectral accelerations, the mainshock produces a higher probability of failure, while at higher spectral accelerations the aftershock is more likely to cause failure.

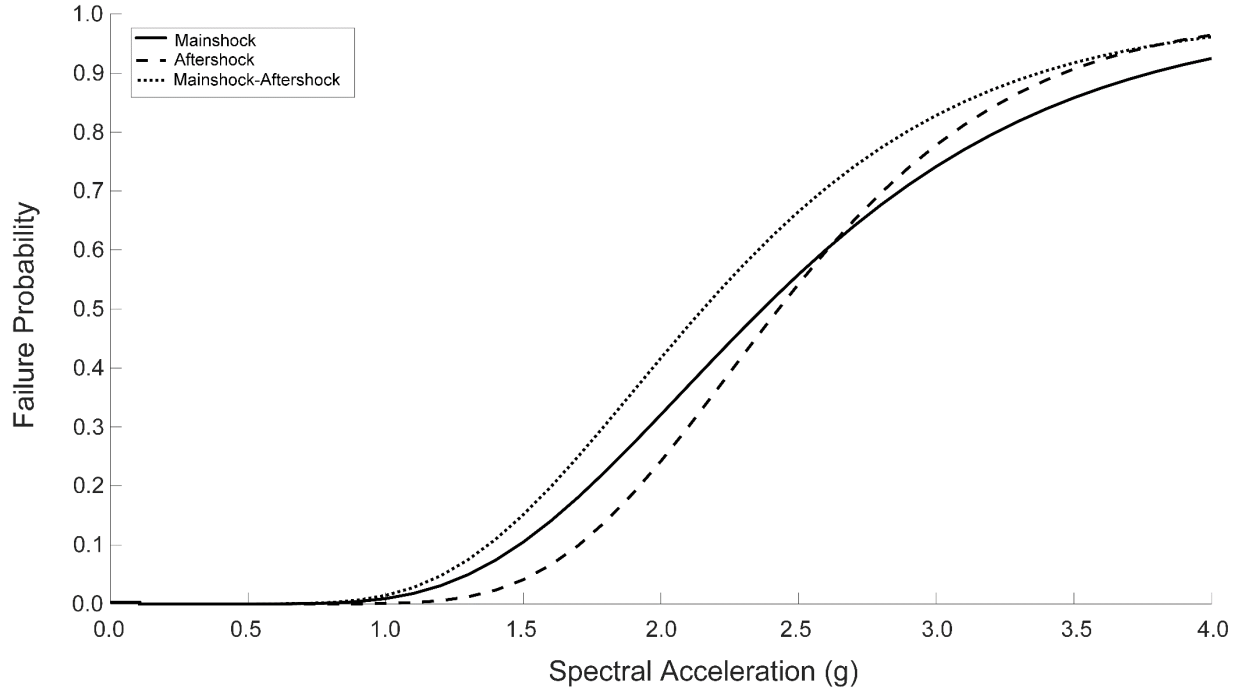

Figure 4-8. Fragility functions for life safety rotation limits of the 50% connection

The 50% connection collapse prevention fragility functions have a failure probability of zero for higher spectral accelerations than those of life safety, with zero probability of failure until approximately 1.0g as opposed to 0.5g of the life safety. This is to be expected as the rotation tolerance is larger for collapse prevention than for life safety. Additionally, as seen in Figure 4-9, the mainshock-aftershock sequence fragility function is shifted the furthest to the left, as predicted, with the mainshock fragility function having a larger failure probability than the aftershock. This indicates that more rotation occurs during the mainshock event than the aftershock event, which is not consistent with the life safety plot that indicates that the aftershock event does produce higher

rotations at larger spectral accelerations. It is important to note, however, that the shifting of the fragilities is a function of the level of damage sustained in the frames during the mainshock and the corresponding period elongation of the frame, which will have an impact of the response during the aftershock.

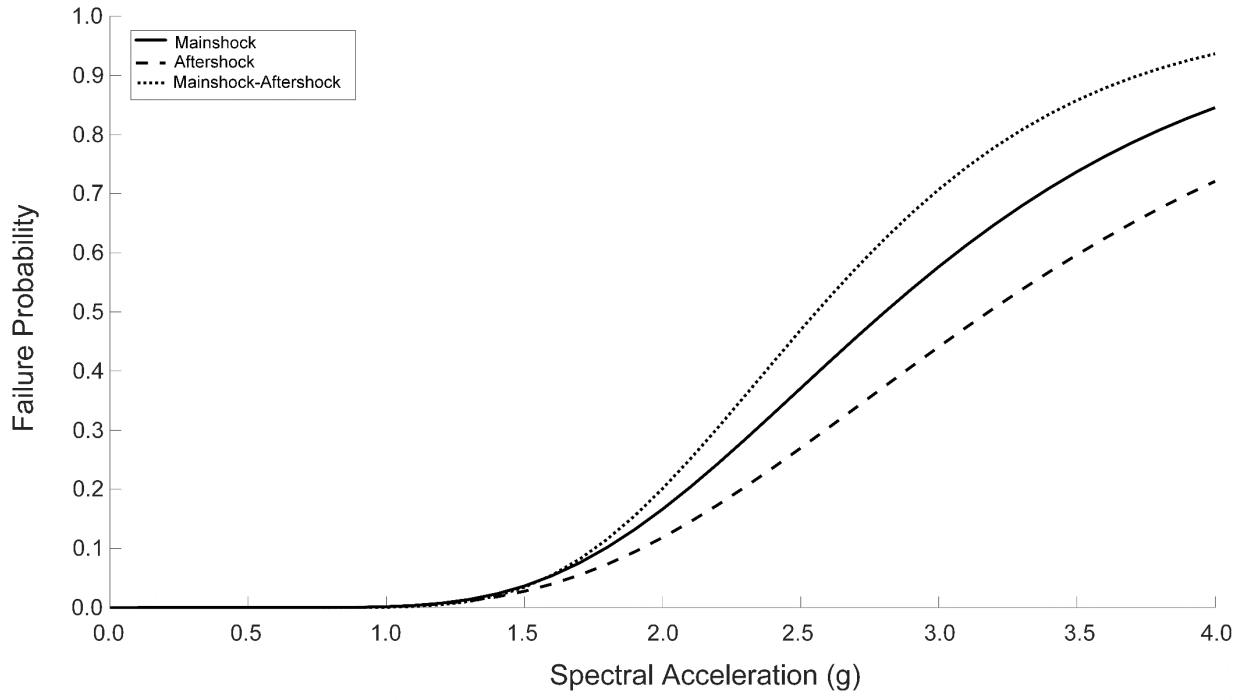

Figure 4-9. Fragility functions for collapse prevention rotation limits of the 50% connection

The probability of strength degradation occurring based upon the rotation limit states set is shown to have the same probability function for both the mainshock and mainshock-aftershock sequence for the 50% connection, seen in Figure 4-10. The aftershock has a lower failure probability at all spectral accelerations. This is consistent with the collapse prevention fragility functions, indicating that the life safety curve is an anomaly, or that there were a large number of aftershock rotations that exceeded the life safety rotation, but did not exceed the collapse

prevention. The strength degradation fragility functions appear to be linearly increasing without asymptotically approaching a failure probability of 1. It is believed that with a higher range of spectral accelerations, the function would approach a value of 1, but larger accelerations were outside of the scope of this work.

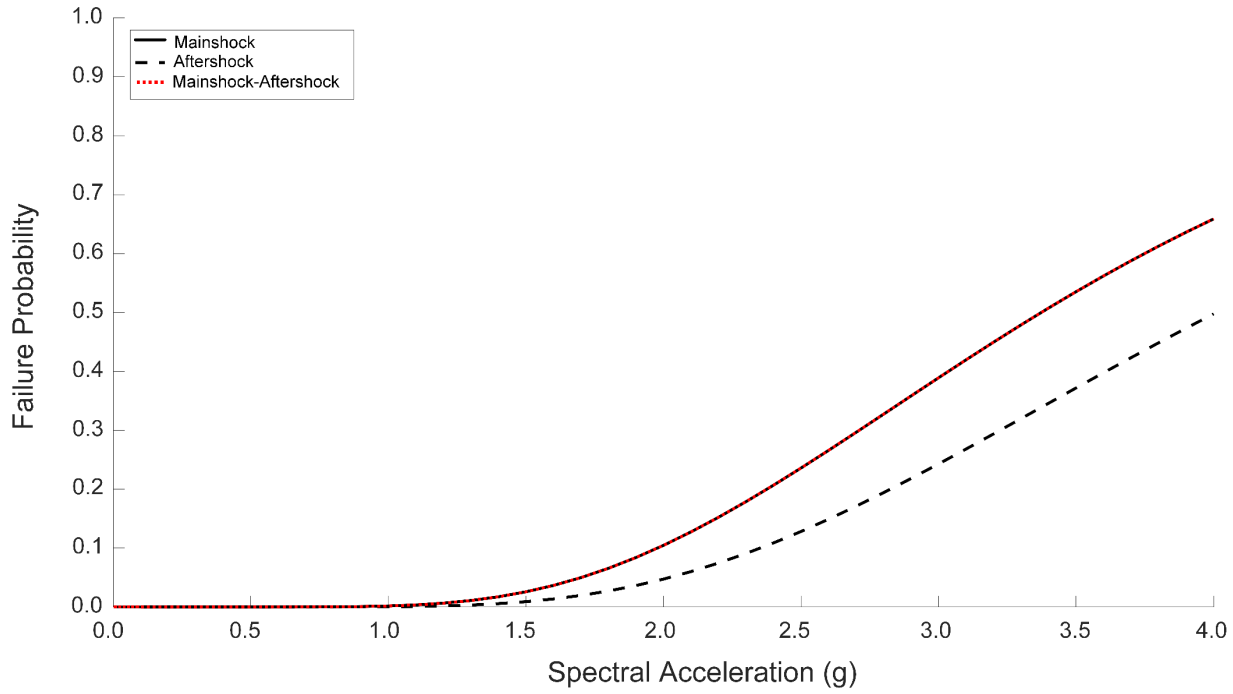

Figure 4-10. Fragility functions for strength degradation of the 50% connection

For the 70% connection, the mainshock produces a higher failure probability throughout all of the investigated spectral accelerations than the aftershock, seen in Figure 4-11. It should be noted that a similar curve behavior to that of some of the column web in shear fragility functions occurred, resulting in the mainshock appearing to have a higher probability of failure than the mainshock-aftershock sequence. This is believed to be due to the nature of the curve fitting

equation and the low failure probabilities and is not reflected in the actual results calculated with the rotation data.

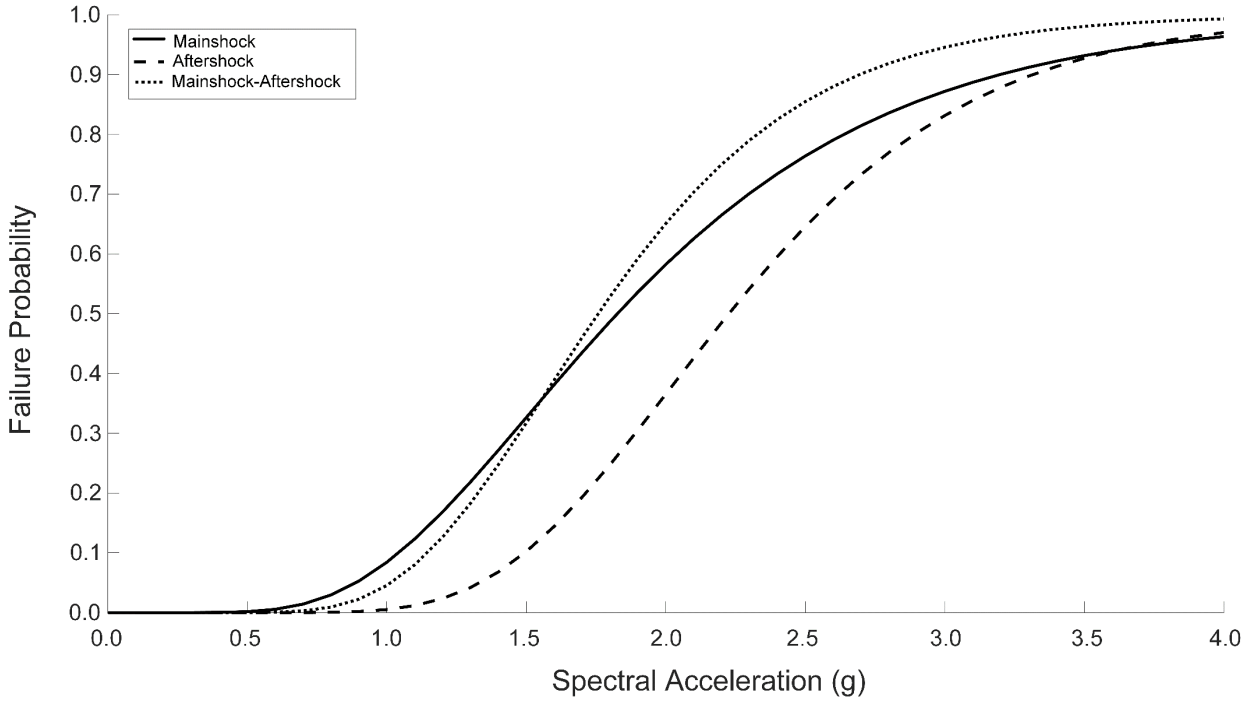

Figure 4-11. Fragility functions for life safety rotation limits of the 70% connection

As with the life safety of the 70% connection, the curve fitting for the collapse prevention indicates that the mainshock event has a higher probability of failure than the mainshock-aftershock event, shown in Figure 4-12. The actual data points do not reflect this, as they are equivalent between the mainshock and mainshock-aftershock but are not reflected in the fragility functions. For the majority of the spectral accelerations, the mainshock is has a higher probability of failure than that of the aftershock, which is consistent with the other fragility function comparisons for rotation limit states.

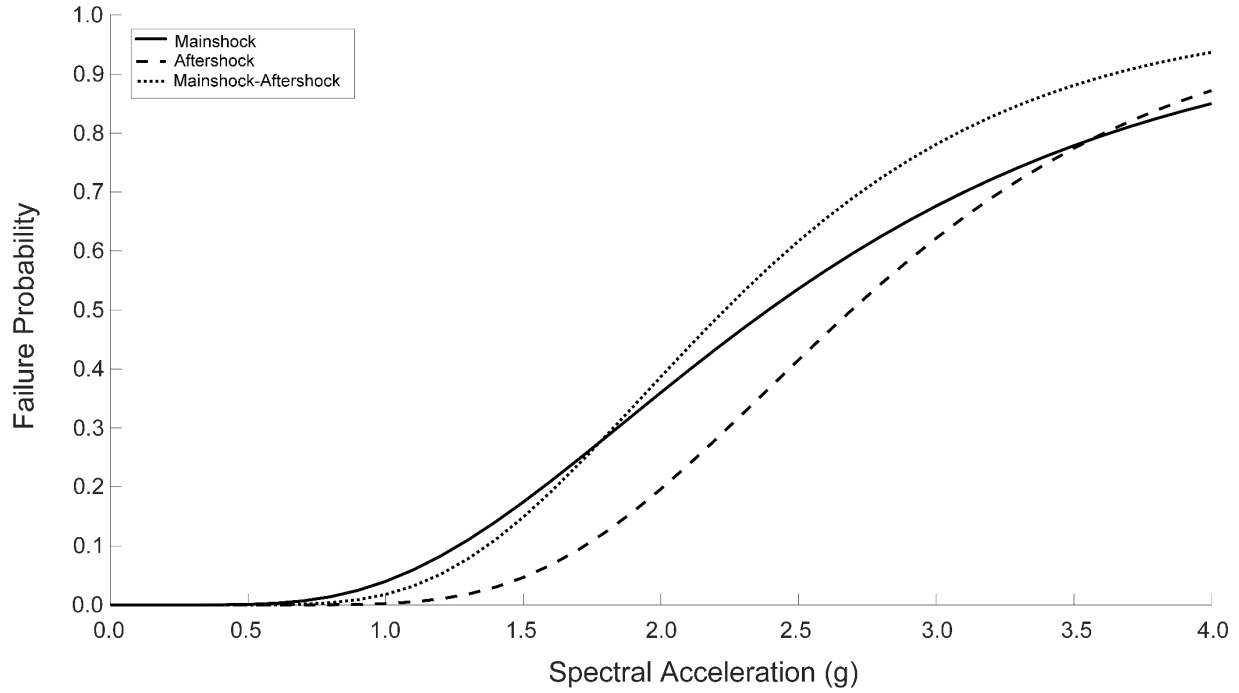

Figure 4-12. Fragility functions for collapse prevention rotation limits of the 70% connection

The strength degradation of the 70% connection shares the same curve fitting behavior as the other two rotation limit states, as seen in Figure 4-13. The same behavior of the mainshock event having a higher probability of failure for the majority of the spectral accelerations under investigation is observed. Additionally, the fragility functions appear to be flatter and not asymptotically approaching a failure probability of 1. As discussed previously, this is believed to be a result of a collection of lower probabilities and would have a different set of curve fitting parameters if more data were produced.

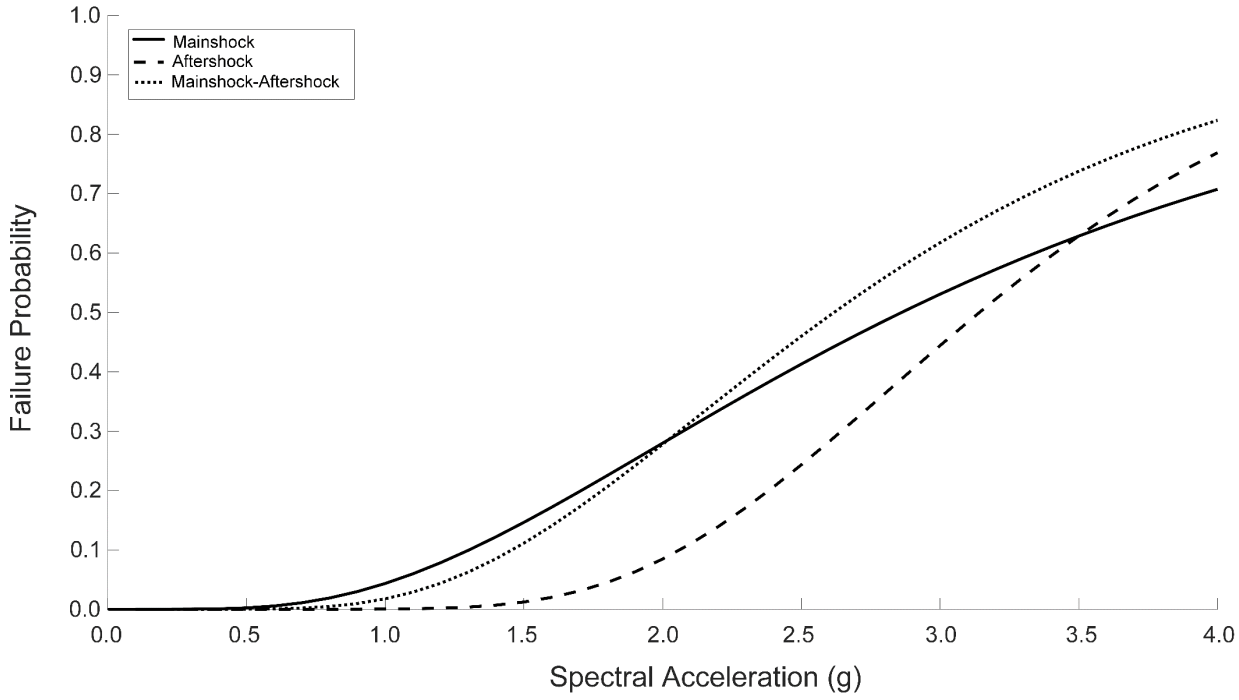

Figure 4-13. Fragility functions for strength degradation rotation limits of the 70% connection

The rotation limit fragility functions are compared between the 50% and 70% connections during the mainshock-aftershock sequence in Figure 4-14. As anticipated, for each of the connections separately, the probability of exceeding the life safety rotation limit is the highest for a given spectral acceleration while exceeding the strength degradation rotation limit is the lowest. Since life safety has the smallest rotation, the connection is most likely to exceed this rotation during ground excitation, while least likely to exceed the strength degradation. However, unlike the bolts in tension and the column web in shear, the 70% connection is more likely to exceed the rotational limit states than the 50% connection. This is consistent with the findings in Admuthe (2018), which discusses the fundamental period of the structure compared with the ground motion period as a reason why the 70% connection is more susceptible to exceeding the rotation limits.

The fundamental period of the moment frame with the 70% connection is much closer to the period of the ground motions than the 50% connection, which causes a larger rotational response.

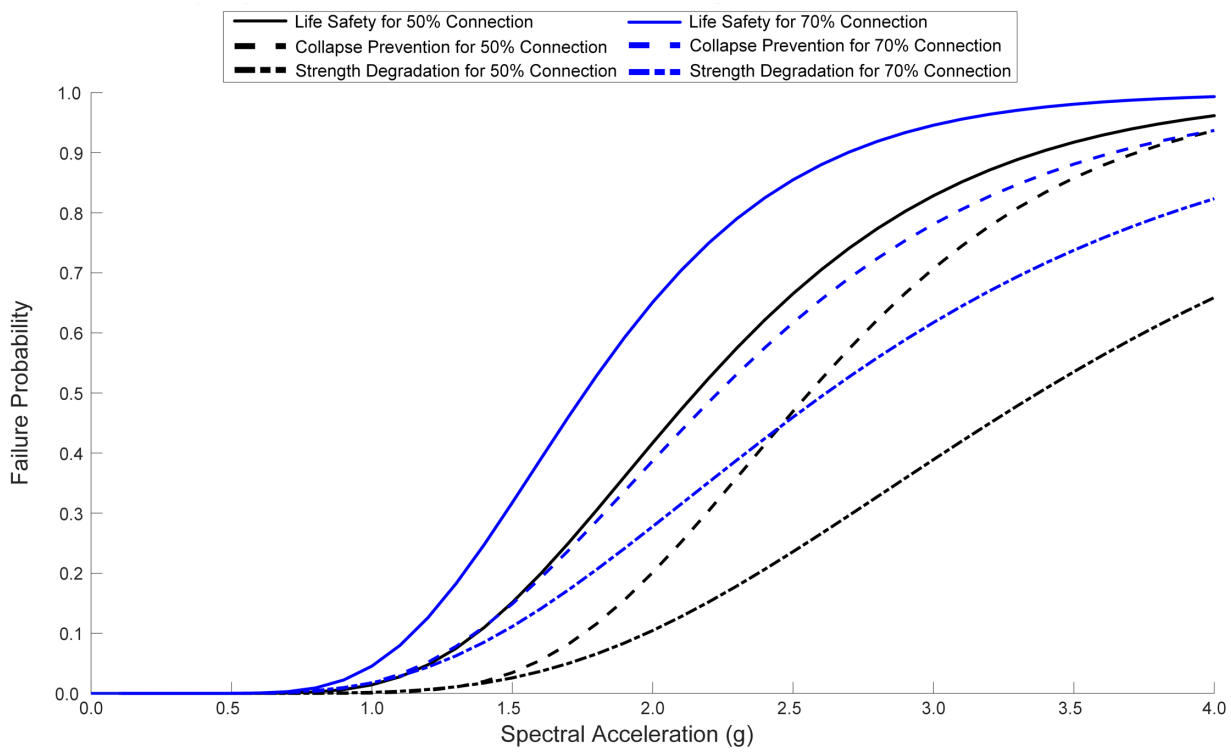

Figure 4-14. Fragility functions for rotation limits during the mainshock-aftershock sequence

Overall, the aftershock motion appeared to have a larger effect on the failure of bolts in tension and the column web failing in shear, while the mainshock appeared to have a larger effect on the exceedance of the rotation limits. Additionally, the connection performed as expected, with the 70% connection having lower probabilities of failure for the column web in shear and the bolts in tension, while also having higher rotation exceedance probabilities.

5 SUMMARY AND CONCLUSIONS

5.1 Summary of Current Work

Extended end-plate connections were modeled using 2D mechanical models with spring elements representing each of the components based upon Eurocode 3 specifications. Two different connection capacities were simulated under mainshock-aftershock ground motion sequences in order to develop fragility functions for the connections. The moment-rotation curves under the ground motions were created using the mechanical models developed in MATLAB for the connections and the necessary moment, rotation, and force data were collected from the analysis. This data was used to develop fragility functions for the extended end-plate connections by comparing the seismic demands on the connection to the limit states outlined in the AISC extended end-plate connection design guide (Murray and Sumner 2003). The fragility functions were developed using the standard lognormal cumulative distribution function equation. Of the limit states assessed, it was determined that bolts failing in tension, the column web failing in shear, and the exceedance of the rotation limits defined for life safety, collapse prevention, and strength degradation occurred.

The fragility functions were compared for the mainshock ground motions, aftershock ground motions, and the mainshock-aftershock sequence of ground motions, to determine the effects of the two separate events in comparison to the combined event. The behavior of the two different strengths of connections were also compared to determine the effects of connection strength on the behavior of the connections under the mainshock-aftershock sequence.

5.2 Conclusions

The following are the main conclusions in this study:

- An understrength factor can be used to correct for the conservatism inherent in the Eurocode 3 based mechanical models.
- The 70% connection had a lower probability of failure for all of the bolt failures in tension and for the column web in shear (strength limit states), while the 50% connection had a lower probability of failure for all of the rotation limit states.
- In most cases, the aftershock event had a higher probability of failure for the strength limit states while the mainshock had a higher probability of exceeding the rotational limits.
- The bolt failures in tension had the largest probabilities of failure, which is consistent with the findings in the AISC extended end-plate design manual and is the most likely mode of failure based upon the failure probabilities of the different limit states.

5.3 Recommendations for Future Studies

In order to better understand the behavior of the connection under mainshock-aftershock sequences, it is recommended that a model that can simulate all fifteen limit states be developed as only seven of the fifteen limit states discussed could be reasonably represented by the mechanical model used in this study.

Additional simulations at higher spectral accelerations would be necessary in order to develop fragility functions for other limit states that did not exhibit failure within the range of spectral accelerations investigated.

Extended end-plate connections are not the only type of bolted connection used in moment-resisting frames. The development of similar fragility curves for top-and-seat angles with double web angle connections and t-stub connections would also be beneficial to understanding the implications of mainshock-aftershock sequences on the behavior of bolted connections.

REFERENCES

Abdelnaby, A. E. (2012). "Multiple Earthquake Effects on Degrading Reinforced Concrete Structures." University of Illinois at Urbana-Champagne.

Abidelah, A., Bouchair, A., and Kerdal, D. E. (2012). "Experimental and analytical behavior of bolted end-plate connections with or without stiffeners." *Journal of Constructional Steel Research*, (76), 13–27.

Admuthe, S. A. (2018). "Semi-rigid steel frames subjected to mainshock-aftershock earthquake sequences." Colorado State University.

Aksoylar, N. D., Elnashai, A. S., and Mahmoud, H. (2011). "The design and seismic performance of low-rise long-span frames with semi-rigid connections." *Journal of Constructional Steel Research*, 67(1), 114–126.

Ang, K. M., and Morris, G. A. (1984). "Anaylsis of Three-Dimensional Frames with Flexible Beam-Column Connections." *Canadian Journal of Civil Engineering*, 11, 245–254.

Attary, N., van de Lindt, J. W., Unnikrishnan, V. U., Barbosa, A. R., and Cox, D. T. (2016). "Methodology for Development of Physics-Based Tsunami Fragilities." *Journal of Structural Engineering, ASCE*, 1–12.

Augusto, H., Castro, J. M., Rebelo, C., and Simões da Silva, L. (2014). "A Contribution To the Extension of the Component Method To Beam-To-Column Connections Subjected To Cyclic Loading." *7th European Conference on Steel and Composite Structures - EUROSTEEL 2014*, 603–604.

Augusto, H., Castro, J. M., Rebelo, C., and Simões da Silva, L. (2016). "Characterization of the Cyclic Behavior of the Web Components in End-plate Beam-to-column Joints." *Procedia*

Engineering, The Author(s), 160(Icmfm Xviii), 101–108.

Baei, M., Ghassemieh, M., and Goudarzi, A. (2012). "Numerical Modelling of End-Plate Moment Connection Subjected to Bending and Axial Forces." *The Journal of Mathematics and Computer Science*, 4(3), 463–472.

Borges, L. (2003). "Probabilistic Evaluation of the Rotation Capacity of Steel Joints." Universidade de Coimbra.

CEN (European Committee for Standardization). (2005). "BS EN 1993-1-8:2005 - Eurocode 3: Design of steel structures - Part 1-8: Design of joints." *Eurocode 3*, Brussels.

Ellingwood, B. R., Celik, O. C., and Kinali, K. (2007). "Fragility assessment of building structural systems in Mid-America." *Earthquake Engineering and Structural Dynamics*, (36), 1935–1952.

Frye, M. J., and Morris, G. A. (1975). "Analysis of Flexibly Connected Steel Frames." *Canadian Journal of Civil Engineering*, 2, 280–291.

Galambos, T. V. (1981). "Load and Resistance Factor Design." *AISC Engineering Journal*, (3), 74–82.

Ghobarah, A., Osman, A., and Korol, R. M. (1990). "Behaviour of extended end-plate connections under cyclic loading." *Engineering Structures*, 12(January).

Girão Coelho, A. M. (2004). "Characterization of the ductility of bolted end plate beam-to-column steel connections." Universidade de Coimbra.

Girão Coelho, A. M., Bijlaard, F. S. K., and Simões da Silva, L. (2004). "Experimental assessment of the ductility of extended end plate connections." *Engineering Structures*, 26(9), 1185–1206.

Girao Coelho, A. M., Simoes da Silva, L., and Bijlaard, F. S. K. (2006). "Ductility analysis of

bolted extended end plate beam-to-column connections in the framework of the component method." *Steel and Composite Structures*, 6(1), 33–53.

Hassan, E. M., and Mahmoud, H. (2018). "A framework for estimating immediate interdependent functionality reduction of a steel hospital following a seismic event." *Engineering Structures*, Elsevier, 168(April), 669–683.

Jaspart, J. P. (2000). "Unified Design Concept for stuctural Joints in Building Frames Application to composite construction.pdf." *Proceedings of the First International Conference on Steel and Composite Structures*, Pusan, 505–514.

Kishi, N., and Chen, W. F. (1990). "Moment-Rotation relations of Semirigid Connections with Angles." *Journal of Structural Engineering*, 116(7), 1813–1834.

Latour, M., Piluso, V., and Rizzano, G. (2011). "Cyclic modeling of bolted beam-to-column connections: Component approach." *Journal of Earthquake Engineering*, 15(4), 537–563.

Leon, R. T., Hu, J. W., and Schrauben, C. (2004). "Rotational Capacity and Demand in Top-and-Seat Angle Connections Subjected To Seismic Loading." *Connections in Steel Structures V: Behaviour, Strength and Design*, 350(4), 201–210.

Li, Q., and Ellingwood, B. R. (2007). "Performance Evaluation and Damage Assessment of Steel Frame Buildings under Mainshock-Aftershock Sequences." *Earthquake Engineering and Structural Dynamics*, 36(3), 405–427.

Li, Y., Song, R., and Van De Lindt, J. W. (2014). "Collapse Fragility of Steel Structures Subjected to Earthquake Mainshock-Aftershock Sequences." *Journal of Structural Engineering*, 140(12), 04014095.

De Lima, L. R. O., De Andrade, S. A. L., Da, P. C. G., and Da Silva, L. S. (2002). "Experimental and mechanical model for predicting the behaviour of minor axis beam-to-column semi-rigid

joints." *International Journal of Mechanical Sciences*, 44(6), 1047–1065.

Lui, E. M., and Chen, W. F. (1986). "Analysis and behaviour of flexibly-jointed frames." *Engineering Structures1*, 8(2), 107–118.

Mahin, S. A. (1980). "Effects of duration and aftershocks on inelastic design earthquakes." *7th World Conference on Earthquake Engineering*, 677–680.

Mahmoud, H. (2011). "Seismic behavior of semi-rigid steel frames." University of Illinois at Urbana-Champaign.

Málaga-Chuquitaype, C., and Elghazouli, A. Y. (2010). "Component-based mechanical models for blind-bolted angle connections." *Engineering Structures*, Elsevier Ltd, 32(10), 3048–3067.

Murray, T. M., and Sumner, E. A. (2003). *Extended End-Plate Moment Connections: Seismic and Wind Applications*. American Institute of Steel Construction.

Porter, K. (2018). *A Beginner's Guide to Fragility, Vulnerability, and Risk*.

Prinz, G. S., Nussbaumer, A., Borges, L., and Khadka, S. (2014). "Experimental testing and simulation of bolted beam-column connections having thick extended endplates and multiple bolts per row." *Engineering Structures*, Elsevier Ltd, 59, 434–447.

Pucinotti, R. (2001). "Top-and-seat and web angle connections: prediction via mechanical model." *Journal of Constructional Steel Research*, 57(6), 663–696.

Richard, R. M., and Abbott, B. J. (1975). "Versatile Elastic-Plastic Stress-Strain Formula." *Journal of Engineering Mechanics*, (101), 511–515.

Ruiz-García, J., and Negrete-Manriquez, J. C. (2011). "Evaluation of drift demands in existing steel frames under as-recorded far-field and near-fault mainshock-aftershock seismic sequences." *Engineering Structures*, 33, 621–34.

SAC. (2000). *Recommended Seismic Evaluation and Upgrade Criteria for Existing Welded Steel Moment-Fram Structures*. Washington D.C.

Del Savio, A. A., Nethercot, D. A., Vellasco, P. C. G. S., Andrade, S. A. L., and Martha, L. F. (2009). "Generalised component-based model for beam-to-column connections including axial versus moment interaction." *Journal of Constructional Steel Research*, Elsevier Ltd, 65(8–9), 1876–1895.

Shaker, F. M. F., and Abd Elrahman, W. M. (2014). "Behavior of flush and extended end-plate beam-to-column joints under bending and axial force." *World Applied Sciences Journal*, 30(6), 685–695.

Simões da Silva, L., Rebelo, C., and Mota, L. (2009). "Extension of the Component Method to End-Plate Beam-to-Column Steel Joints subjected to Seismic Loading." *Trends in Civil and Structural Engineering Computing*, Saxe-Coburg Publications, Stirlingshire, Scotland, 149–167.

Simões da Silva, L., Shahbazian, A., Gentili, F., and Augusto, H. (2016). "Implementation of a component model for the cyclic behaviour of steel joints." *Connections in steel structures VIII*, Boston.

Song, R., Li, Y., and van de Lindt, J. W. (2014). "Impact of earthquake ground motion characteristics on collapse risk of post-mainshock buildings considering aftershocks." *Engineering Structures*, Elsevier Ltd, 81, 349–361.

Swanson, J. A., and Leon, R. T. (2000). "Bolted Steel Connections: Tests on T-Stub Components." *Journal of Structural Engineering*, 126(1), 50–56.